






Development and structure elucidation of new VO^{2+} , Mn^{2+} , Zn^{2+} , and Pd^{2+} complexes based on azomethine ferrocenyl ligand: DNA interaction, antimicrobial, antioxidant, anticancer activities, and molecular docking

Enas T. Aljohani¹  | Mohamed R. Shehata²  | Fatmah Alkhatib³  |
Seraj Omar Alzahrani⁴  | Ahmed M. Abu-Dief^{4,5} 

¹Chemistry Department, College of Science, Majmaah University, Majmaah, Saudi Arabia

²Chemistry Department, Faculty of Science, Cairo University, Giza, Egypt

³Chemistry Department, Faculty of Applied Science, Umm Al-Qura University, Makkah, Saudi Arabia

⁴Chemistry Department, College of Science, Taibah University, Madinah, Saudi Arabia

⁵Chemistry Department, Faculty of Science, Sohag University, Sohag, Egypt

Correspondence

Ahmed M. Abu-Dief, Chemistry Department, College of Science, Taibah University, Madinah, P.O. Box 344, Saudi Arabia.

Email: ahmed_benzoic@yahoo.com; amamohammed@taibahu.edu.sa

An organometallic azomethine ferrocenyl ligand (FCAP) and its transition metal complexes ($[\text{M}(\text{FCAP})_2]$, where $\text{M} = \text{VO}^{2+}$, Mn^{2+} cations, and $[\text{M}(\text{FCAP})(\text{CH}_3\text{COO}^- \text{ or } \text{NO}_3^-)]$, where $\text{M} = \text{Zn}^{2+}$ and Pd^{2+} cations) were prepared. Their structures were confirmed via various spectral and physico-chemical studies performed. The crystallinity of the investigated metal chelates was confirmed by X-ray diffraction data. The spectral data of the FCAP azomethine ligand and its metal chelates were explained concerning the structural changes due to complex formation. From the electronic spectra and the magnetic moments, the information about geometric structures can be concluded. The activation thermodynamic parameters of the thermal degradation for FCAP complexes were calculated utilizing the method of Coats–Redfern. *in vitro* antimicrobial, anticancer, and antioxidant activities of FCAP azomethine ligand and its complexes were screened. All the investigated metal chelates exhibited superiority on the free FCAP ligand in successful treatment. Moreover, the binding nature of the investigated complexes with calf thymus DNA (ctDNA) was examined by various methods such as spectrophotometry, viscosity, and, gel electrophoresis. Their binding feature to ctDNA was proposed to be electrostatic, intercalation, or replacement mode. Furthermore, molecular docking inspection has been conducted to clarify the nature of the binding and binding affinity of protein synthesized compounds (PDB:3hb5).

KEYWORDS

computational studies, ferrocene-derived azomethine ligand, metal (II) chelates, molecular docking, organometallic-based antimicrobials

1 | INTRODUCTION

Cancer is deemed as a large class of diseases that includes the growth of abnormal cell that may be dispersed to other parts of the body. Many medications used for cancer remediation are now cytotoxic, affecting DNA activity

in cells in one way or more. As a result, designing novel anticancer drugs with high efficacy and low toxicity is the most critical challenge these days.^[1–5] For their lipophilic, non-toxic, and reversible redox properties and their stability in a biological medium, ferrocene derivatives are of importance among metallocenes.^[6] These

compounds have many material science applications, including electroactive materials, catalysts, sensors, and aerospace materials, because of the favorable electronic properties of ferrocene derivatives and their simple functionalization.^[7–10] Ferrocenyl transition metal compounds have recently been found in molecular sensors, molecular switches, molecular ferromagnets, electrochemical agents, and liquid crystals.^[11–14] Bio-organometallic chemistry has therefore gained a great deal of research attention as a new field. A connection between organometallic chemistry and molecular biotechnology is established by ferrocenyl linked to transitional metal compounds. In the development of new therapeutic reagents and DNA molecular probes, binding studies of small molecules to DNA are very important.^[15–18] DNA binding potential is the dominant attitude tested in pharmacology to speculate on the anticancer potential of novel compounds. Consequently, it is important to design tiny compounds that bind and interact strongly with DNA. In the interaction of complexes with DNA molecules, the nature of the ligand and metal ion is of vital importance, which helps to design novel drugs and create new selective, effective DNA recognition and cleaving agents. The relationship between the transition metal complexes and DNA has therefore been thoroughly investigated.^[19–23]

We wish to report here FCAP ferrocene azomethine ligand and its use in the preparation, of V (IV)O, Mn (II), Pd (II), and Zn (II) ferrocene azomethine chelates. Moreover, we will make structure elucidation for the prepared compounds utilizing different physicochemical and analytical tools. In addition, we will check the possibility of DNA interaction of the investigated ferrocene azomethine chelates. Furthermore, their application as a class of organometallic-based antimicrobial, anticancer, and antioxidant agents will be screened.

2 | PROTOCOLS OF EXPERIMENTS

2.1 | Materials and methods

All solvents used were of a chromatographic grade. Organic compounds such as ferrocene carboxaldehyde and 2-amino phenol and metal salts such as manganese chloride ($\text{MnCl}_2 \cdot 4\text{H}_2\text{O}$), zinc (II) nitrate ($\text{Zn}(\text{NO}_3)_2 \cdot 4\text{H}_2\text{O}$), vanadyl acetylacetonate ($\text{V}(\text{acac})_2$), and palladium acetate ($\text{Pd}(\text{CH}_3\text{COO})_2$) were purchased from Sigma-Aldrich. C, H, and N contents were determined using a CHNS-932 (LECO) Vario elemental analyzer. DMSO- d_6 reported ^1H and ^{13}C NMR spectra on a JEOL AL-300 FT-NMR multinuclear spectrometer. The Shimadzu UV-3600 UV-vis-NIR spectrophotometer was

used to acquire the electronic spectra of the investigated compounds. Infrared (IR) spectra on a Perkin Elmer FT-IR spectrophotometer in the $400\text{--}4,000\text{ cm}^{-1}$ area were registered in KBr. The molar conductivity of solid complex solutions was measured using the Jenway 4010 conductivity meter. Thermogravimetric (TGA) analyses of solid complexes were carried out using a thermal analyzer of Shimadzu TG-50H from room temperature to $1,000^\circ\text{C}$.

2.2 | Ligand preparation method

Organometallic azomethine FCAP ligand was prepared by using the homogeneous solution of 2-amino phenol (2 mmol, 0.218 g) with ferrocene carboxaldehyde (2 mmol, 0.428 g). These compounds were separately dissolved in absolute ethanol, stirred on hot magnetic hot plate for 45 min, and refluxed using a water condenser for 1 h. After complete reflux, the reaction mixture is cooled at room temperature and kept overnight in a dark place, the solid separated, and the yield of product is 88%.

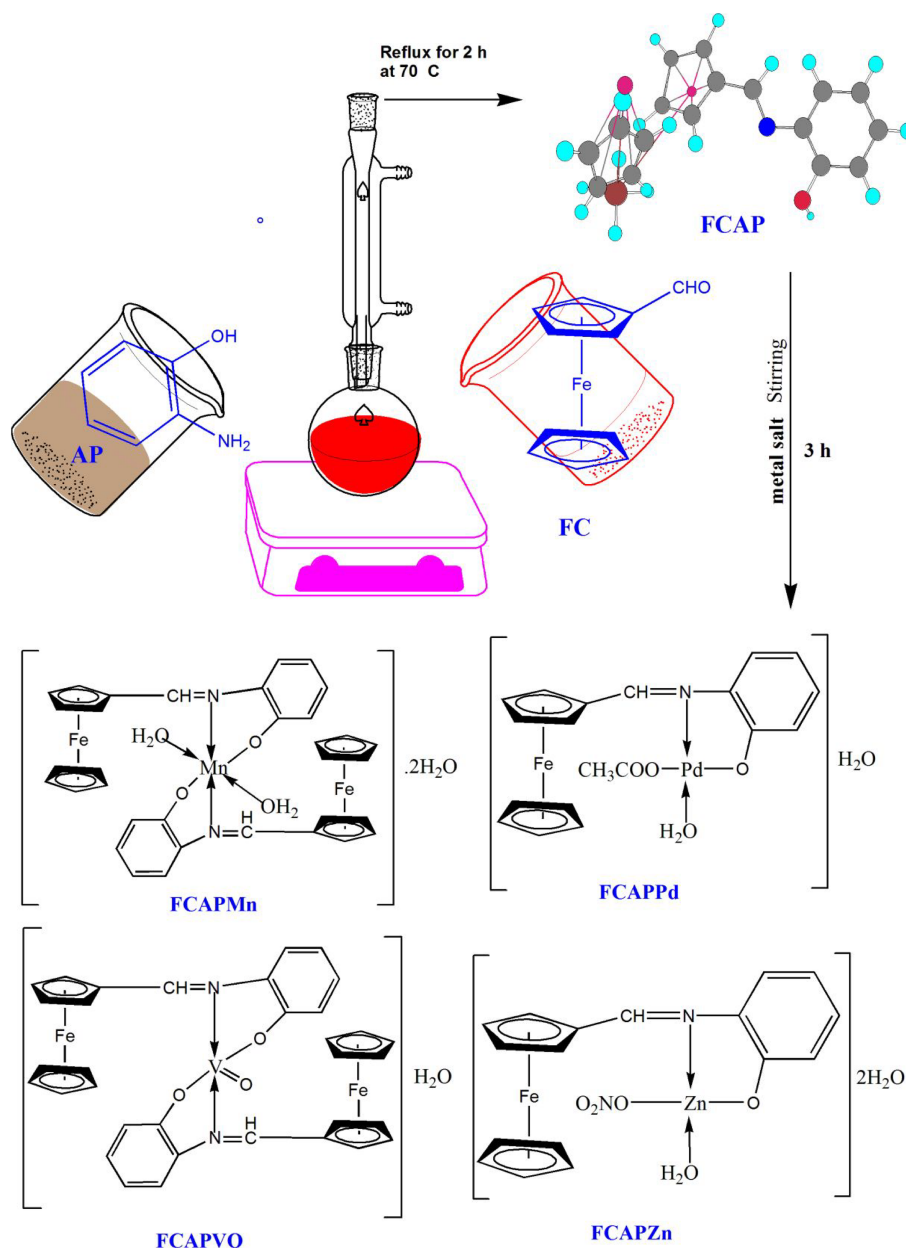
2.3 | Azomethine FCAP metal chelate preparation

FCAP azomethine complexes were prepared by mixing equimolar of ethanolic solution of FCAP azomethine ligand (2 mmol, 0.610 g) with 2 mmol of $\text{Zn}(\text{NO}_3)_2 \cdot 4\text{H}_2\text{O}$ (0.58 g), $\text{Pd}(\text{CH}_3\text{COO})_2$ (0.448 g) or 1 mmol of $\text{VO}(\text{acac})_2$ (0.54 g) or $\text{MnCl}_2 \cdot 4\text{H}_2\text{O}$ (0.19 g). The resulted mixtures were refluxed for 2 h, and then, the reaction mixture is cooled at room temperature. By filtration, the solid compounds have been separated, washed several times with hot ethanol and ether, and dried over CaCl_2 . In monitoring the developed compounds' purity, thin layer chromatography (TLC) was used. Synthetic pathway of the azomethine FCAP ligand and its complexes are given in Scheme 1.

2.4 | Computational studies for molecular optimization

The lowest energy geometries, using the density functional theory (DFT) and the Gaussian09 software, were measured. The DFT/B3LYP/LANL2DZ theory level was used. For the optimization of geometry to achieve the lowest energy structures for FCAP ferrocenyl imine ligand and its VO^{2+} , Mn^{2+} , Zn^{2+} , and Pd^{2+} complexes.

SCHEME 1 Diagrammatic scheme for pathway of synthesis of the investigated FCAP imine ligand and its metal chelates



2.5 | Reactivity with ctDNA

Calf thymus DNA (ctDNA) stock solution was freshly prepared in Tris-HCl (Tris(hydroxymethyl)aminomethane hydrochloride) (5.0 mM) and NaCl (50.0 mM) in aqueous media and then adjusted at pH = 7.5 and stored at 4 °C for 4 days according to the standard method.^[3,4,19] The absorbance of ctDNA stock solution was detected at 260 nm (UV region) and the molar absorptivity coefficient (ϵ) was found to be $6,600 \text{ mol}^{-1} \text{ cm}^{-1}$. Consequently, for the stock solution of ctDNA, it is important that the ratio of UV absorbance at 260 and 280 nm, A_{260}/A_{280} , be >1.8 because it is indicative that the ctDNA solution is sufficiently free of protein.^[24,25] Ethidium bromide (EB) was used as a standard and its concentration was

spectrophotometrically determined at 480 nm ($5,860 \text{ mol}^{-1} \text{ cm}^{-1}$). Stock solutions of metal complexes (FCAPZn, FCAPPd, FCAPMn, and FCAPVO) were prepared in fresh dimethyl sulfoxide (DMSO). ctDNA interaction with FCAPZn, FCAPPd, FCAPMn, or FCAPVO complex was monitored by the control of pH with the progressive addition of $1.0 \times 10^{-3} \text{ mol dm}^{-3}$ from ctDNA at pH = 7.5.

2.5.1 | UV-vis spectrophotometric titration

UV-vis spectra were obtained at different [ctDNA] concentrations added to given [FCAPZn], [FCAPPd],

[FCAPMn], or [FCAPVO] concentrations in fresh DMSO according to known method.^[3,4,19] The absorbance values of ctDNA were measured concerning blank solution that includes all additions except the tested compound. The binding constant (K_b), which represents interaction strength of each tested compound with ctDNA, was obtained from Equation 1.^[24–27]

$$\frac{[\text{DNA}]}{\varepsilon_a - \varepsilon_f} = \frac{[\text{DNA}]}{\varepsilon_b - \varepsilon_f} + \frac{1}{[K_b(\varepsilon_b - \varepsilon_f)]}, \quad (1)$$

where the molar absorptivity of unreacted, partial, and complete reacted binding of ctDNA with checked compounds (FCAPZn, FCAPPd, FCAPMn, or FCAPVO) are ε_f , ε_a , and ε_b , respectively. The molar absorptivities (ε_a and ε_b) were extracted from plots of A_{abs} against [compound] or ctDNA concentrations [DNA], respectively. K_b values were estimated from intercept/slope ratio of the plots. ΔG_b° (standard Gibb's free energy) that assigned for interaction of ctDNA with FCAPZn, FCAPPd, FCAPMn, or FCAPVO complex was determined from Equation 2^[28]:

$$\Delta G_b^\circ = -RT \ln K_b. \quad (2)$$

The chromism values could be determined through Equation 3:

$$\text{chromism, \%} = \frac{A_{\text{free}} - A_{\text{bonding}}}{A_{\text{free}}}, \quad (3)$$

where A_{free} is the absorbance of free compounds (FCAPZn, FCAPPd, FCAPMn, or FCAPVO) and A_{bonding} is the absorbance of each complex with alternative ctDNA concentrations at λ_{max} .

2.5.2 | Hydrodynamic reactions (viscosity method)

The Oswald microviscometer was used to evaluate the relative viscosities of interacted compounds. Hence, evaluation for hydrodynamic interaction between current compounds (FCAPZn, FCAPPd, FCAPMn, or FCAPVO) with ctDNA at room temperature was performed according to reported method.^[17–19] In the presence and absence of ctDNA under inert N_2 gas bubbling conditions, the fluidity time (s) for different complex concentrations (from 5.0 to 50.0 μM) could be calculated by applying it in Equation 4^[29]:

$$\eta = \frac{t - t^\circ}{t^\circ}, \quad (4)$$

where t is the fluidity time for the compounds and ctDNA, whereas t° is the total time of fluidity of complex. The relative values of viscosity (η/η°) were estimated from plot of viscosity against $1/R$. R values could be deduced from Equation 5:

$$R = \frac{[\text{DNA}]}{[\text{Compound}]}. \quad (5)$$

[DNA] is the molar concentration of ctDNA, whereas [compound] is the molar concentration of the complex.

2.5.3 | Electrophoresis of agarose gel

Electrophoresis of agarose gel is considered an efficient method for studying the degradation effect of the compound tested in ctDNA.^[30] A stock solution of 20.0 mg of FCAPZn, FCAPPd, FCAPMn, or FCAPVO complex in dimethylformamide (DMF; 20.0 ml) was prepared. The 25.0- μM complex was then combined with extracted DNA (from ctDNA) and kept for 1 h at 37°C for incubation. A mixture sample (30.0 μl) was then taken and poured into an equimolar ratio of 1:1 bromophenol blue dye and then moved to the electrophoresis chamber wells. This is in parallel with the regular pure DNA marker sample in the TBE buffer solution, that is, 50-mM Tris-base at pH 7.2 combined with 1.0-mM ethylenediaminetetraacetic acid (EDTA)/1.0 L. Gel running was tracked by adding 60 V to the electrophoresis chamber for ~ 45 min.^[18,30] By taking images with the Panasonic DMC-LZ5 Lumix genius 3, the agarose gel is recorded in ctDNA gel.^[18,30]

2.6 | Biological assay: Antibacterial and antifungal activities

As discussed in our previous publications, in vitro antifungal and antibacterial activities of FCAP ligand and its metal chelates were evaluated by the well diffusion method.^[21–25] Antifungal action of the investigated ferrocenyl azomethine chelates was tested for the inhibition of *Aspergillus flavus*, *Getrichm candidum*, and *Fusarium oxysporum* fungi, and antibacterial activity was checked on *Serratia marcescense*, *Escherichia coli*, and *Micrococcus luteus* bacteria. Ofloxacin and fluconazole have been taken as a standard for the testing of bacterial and fungal action. To ensure precision, all the measurements were reported in duplicate for the ligand and the complexes.

2.6.1 | MIC and index of activity (A)

A number of different FCAP, FCAPZn, FCAPPd, FCAPMn, and FCAPVO concentrations were tested for minimum inhibitory concentration (MIC) determination of their antimicrobial potential. Clear inhibition zones were appeared and measured in millimeter, and the activity index percent were calculated as from Equation 6^[31]:

$$A = \frac{\text{inhibition zone (mm)}}{\text{standard drug inhibition zone (mm)}} \times 100. \quad (6)$$

2.7 | DPPH activity of free radical scavenging

The free radical scavenging screening of FCAP, FCAPZn, FCAPPd, FCAPMn, and FCAPVO compounds was examined with the scavenging of DPPH radical. The decay in the purple color of the methanolic solution of DPPH to pale yellow color was followed spectroscopically. A 2.40-ml methanol of 0.1-mM DPPH was dropwisely poured to an aqueous solution of 100-μM FCAP, FCAPZn, FCAPPd, FCAPMn, or FCAPVO. The resulted mixed solution was vortexed in a dark atmosphere for a half hour (25°C). Measuring of the molar absorptivity of the resulted solution at $\lambda = 517$ nm was achieved spectrophotometrically. Involving vitamin C, that is, ascorbic acid, was important for a positive control.^[4] Methanol and a blank sample (without DPPH) were also performed for comparative negative monitoring. The capacity of DPPH radical screening percentages was predestined within Equation 7:

$$\% \text{ Reduction of absorbance} = [(a - b)/a] \times 100, \quad (7)$$

where a is the blank sample absorption and b is the checked sample absorption.

2.8 | Anticancer activity

Anticancer properties of newly synthesized FCAP, FCAPZn, FCAPPd, FCAPMn, or FCAPVO were evaluated spectrophotometrically against hepatocellular carcinoma (HepG-2), breast adenocarcinoma (MCF-7), and colon carcinoma (HCT-116) cell lines. Such was done by employing sulforhodamine B (SRB) stain assay according to reported method.^[10] Enzyme-linked immunosorbent assay (ELISA) microplate reader (Meter tech. Σ 960, "USA") was used to record absorbance at 564 nm. Cells were seeded in 96-multiwell plates, 10^4 cells/well,

and serial dilutions were applied by using tested compounds. Cells were incubated at 37°C for 48 h under 15% (v/v) CO₂-humidified atmosphere, and then, SRB was applied. Vinblastine was used as the standard and the corresponding IC₅₀ values were determined in Equation 8^[32]:

$$IC_{50}(\%) = \frac{\text{Control}_{OD} - \text{Compound}_{OD}}{\text{Control}_{OD}} \times 100. \quad (8)$$

3 | FINDINGS AND DISCUSSION

3.1 | Description

The traditional condensation method was used to synthesize the ferrocenyl complexes studied. Physicochemical properties of the titled azomethine organometallic ligand and its V (IV)O, Mn (II), Pd (II), and Zn (II) chelates were given in Table 1. All of the complexes are colored and thermally stable at room temperature. The titled azomethine organometallic compounds were soluble in absolute alcohol, DMF, and DMSO but were insoluble in organic solvents like on non-polar organic solvents such as benzene and toluene.

3.2 | ¹H NMR spectra and vibrational properties data

The FCAP ligand HNMR spectrum shows a proton signal of CH=N at 9.60 ppm. Ferrocene protons may be associated with multiple signals observed in the 4.80–4.27 ppm range.^[33] These signals appeared almost in the same range in the FCAPPd and FCAPZn complexes. The aromatic protons of the benzene ring were allocated to multiple signals within the range of 6.00–7.11 ppm.^[34] At 8.75 ppm, a single signal appeared linked to the phenolic proton that disappeared in the complexes of FCAPPd and FCAPZn. The free ligand IR spectra vary from those of their complexes and provide important indications about the ligand binding sites. In comparison with its FCAPPd, FCAPZn, FCAPMn, and FCAPVO complexes, the experimentally observed IR (Fourier transform [FT]-IR) peaks of the organometallic ferrocenyl FCAP imine ligand are recorded in Table 1. The IR spectra of the FCAP ligand and its FCAPPd complex are given in Figure S1, as typical examples. The change in the functional groups' wavelength range indicates that complexes are formed with metal ions and ligand. It was inferred from the data that all complexes showed a substantial shift in the $\nu(\text{C}=\text{N})$ (azomethine) band from higher ($1,593 \text{ cm}^{-1}$) to lower

TABLE 1 Analytical and physical properties beside IR spectral bands for the prepared FCAP ferrocenyl azomethine ligand and its metal chelates

Compounds	Empirical formula (formulae weight)	Color	M. p. and decomp. temp. (°C)	Λ_m (Ω^{-1} cm ² mol ⁻¹)	μ_{eff} (B.M.)	Analysis (%) found (calc.)				IR (cm ⁻¹)			
						C	H	N		$\nu(\text{OH})/\text{H}_2\text{O}$	$\nu(\text{C}=\text{N})$ (vs)	$\nu(\text{C}-\text{O})_{\text{ph}}$	$\nu(\text{M}-\text{O})$ $\nu(\text{M}-\text{N})$
FCAP	C ₁₇ H ₁₅ FeNO (305.15)	Deep red	175	-	-	66.78 (66.91)	4.99 (4.95)	4.53 (4.59)		3,416	1,597	1,278	...
FCAPVO	[V(C ₃₄ H ₃₀ Fe ₂ N ₂ O ₄)] 693.24	Deep brown	>300	11.30	1.81	59.05 (58.91)	4.32 (4.36)	4.09 (4.04)		3,338	1,579	1,275	581
FCAPPd	[Pd(C ₁₉ H ₂₁ FeNO ₅)] 505.64	Deep brown	>300	8.45	Diamagnetic	45.17 (45.13)	4.16 (4.19)	2.81 (2.77)		3,424	1,570	1,272	585
FCAPMn	[Mn(C ₃₄ H ₃₆ Fe ₂ N ₂ O ₆)] 735.29	Deep brown	>300	14.20	5.43	55.61 (55.54)	4.88 (4.93)	3.87 (3.81)		3,335	1,571	1,273	558
FCAPZn	[Zn(C ₁₇ H ₂₀ FeN ₂ O ₇)] 485.58	Deep brown	>300	9.70	Diamagnetic	42.11 (42.05)	4.12 (4.15)	5.84 (5.77)		3,421	1,576	1,273	588

Abbreviation: IR, infrared.

(1,570–1,579 cm⁻¹) frequencies, confirming its coordination with metal ion.^[35] The observed peaks in the spectra of the complexes in the region between 558–588 cm⁻¹ and 436–468 cm⁻¹ belong M-O, M-N vibrational modes and confirms the coordination of the azomethine group to the investigated cations.^[36]

In the FCAPZn complex, the characteristic frequencies of the coordinated nitrate group have three non-degenerate modes at 1,461 cm⁻¹ (NO₂)_{asy}, 1,348 cm⁻¹ (NO₂)_{sy}, and 845 cm⁻¹ (NO). The difference between the two highest frequency bands ($\nu = \nu_{\text{asy}} - \nu_{\text{sy}}$) is 113 cm⁻¹, implying that nitrate ion (NO₃) in the solid complex coordinates to Zn (II) ion in a unidentate manner.^[22] The FCAPVO complex displays an additional band at 939 cm⁻¹ due to the V = O frequency, in addition to the other bands.^[2] Two strong to medium bands were identified at 1,540 and 1,320 cm⁻¹ for the prepared FCAPPd complex that could be assigned (asyCOO⁻) and (syCOO⁻) vibrations of the acetate group carboxylate ion. The difference between the vibrations of asymmetric and symmetric stretching vibration [(asyCOO⁻) – (syCOO⁻)] was found to be 210 cm⁻¹, which corresponds to monodentate ligation.^[5]

3.3 | Elemental analyses and molar conductivity measurements

The physical characterization data, microanalytical data, and values of molar conductance for the investigated complex samples are entered in Table 1. Each value corresponds to the above samples found to be in good agreement with the deduced molecular composition including FCAP ligand and its complexes. Due to the synthesized complexes being non-electrolytic, the DMF solution of these metal complexes shows lower molar conductance values (8.45–14.20 Ω^{-1} mol⁻¹ cm²) that represent the absence of anion in the outer sphere of the complexes.^[37,38]

3.4 | Electronic spectra and magnetic moment measurements

The FCAP UV–vis absorption spectra in EtOH are compatible with most ferrocenyl chromophores in which they demonstrate two charge transfer bands (cf. Figure 1 and Table S1). For the investigated compounds, the spectra contain a prominent absorption band with a maximum of 237–252 nm that can be ascribed to a high-energy ligand-based electronic transition $\pi-\pi^*$. In addition, the absorption band in the visible region is observed at 352 nm, which is assigned to the intraligand band of

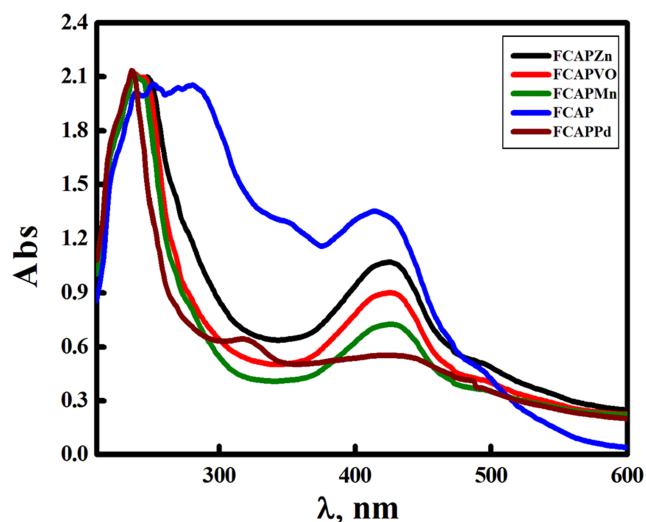


FIGURE 1 Comparable spectral electronic scans of FCAP ligand and its FCAPZn, FCAPPd, FCAPMn, and FCAPV complexes in ethanol media at 25°C

FCAP compound. In addition, the absorption band observed within the region of 413–426 nm could be ascribed to the metal–ligand charge transfer (MLCT) process.^[39] The weak d-d transitions in the Schiff bases were observed within the region of 485–493 nm.

The magnetic moment (μ_{eff}) of titled metal azomethine chelates, shown in Table 1, is 1.81 for V (IV)O. This value indicates that the FCAPVO complex with a square pyramidal geometry is paramagnetic,^[40] where the FCAPMn complex is paramagnetic with μ_{eff} of 5.43, indicating octahedral structure. Diamagnetic behavior with zero μ_{eff} value of FCAPZn and FCAPPd complexes suggests that they have tetrahedral and square planar geometry, respectively.^[41]

3.5 | Powder X-ray diffraction analysis for the investigated FCAP complexes

Single crystal growth of synthesized compounds from different solvents, including ethanol, methanol, chloroform, acetonitrile, and DMF, does not achieve single crystal growth. However, the subtle crystalline nature of compounds is obtained, which is not sufficient for single crystal studies and is thus used to measure the degree of compound crystallinity. In order to gain more information about the formation of complexes and the structure of complexes, X-ray diffraction was carried out. The X-ray diffractogram of synthesized complexes (see Figure 2) was scanned at wavelength 1.5406 Å in the range 5–100° (θ),

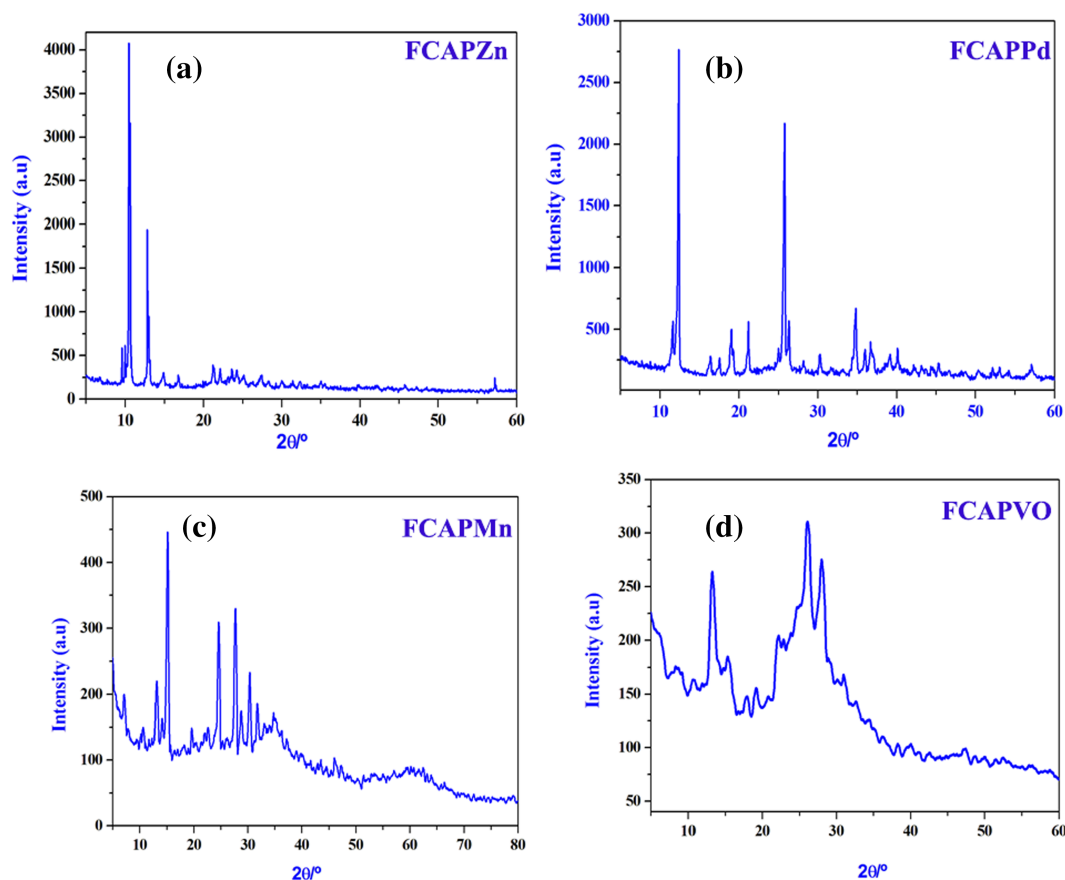


FIGURE 2 Powder X-ray pattern for the prepared FCAP complexes

which gives the essence of their crystallinity. The powder XRD patterns display the crystalline character of the complexes, as shown in Figure 2. The presence of crystallinity in the organometallic Schiff base complexes is due to the metallic compounds' intrinsic crystalline nature.^[42]

3.6 | TGA and its kinetic aspects of the investigated organometallic FCAP complexes

The thermal decomposition method of the metal complexes was analyzed using the TGA technique, and the thermokinetic parameters were estimated. The temperature ranges, number of stages, stages of degradation, degradation product loss, the calculated and found weight loss percentage, and finally, the residues of all compounds were given in Table 4. On heating of the FCAPMn complex within the temperature range 35–120°C, two hydration molecules of water with a mass loss = 4.93% (calc. = 4.90%) (cf. Figure S2) were liberated. The second step was the loss of two coordinated water molecules at 122–180°C with a mass loss = 4.86% (calc. = 4.90%). The third and fourth steps were observed within the range 182–370°C, corresponding to the loss of part of the ligand with a formula $C_{20}H_{18}$ with a mass loss = 35.06% (calc. = 35.14%). The fifth and six stages were carried out within the range 372–535°C, corresponding to the loss of $C_{14}H_{10}N_2O_2$ fragment leaving mixture of MnO + 2FeO as residue. The same behavior was observed for the rest of the complexes as shown in Table 2. The data obtained from TGA were correlated with CHN and confirmed the suggested formula for the prepared complexes.

Kinetic and thermodynamic parameters were calculated for all tested complexes over all degradation steps. The obtained values were aggregated (Table 2) and reveal the following notices.

1. The higher the activation energy values, the higher the stability of the compound except the first step. Such a step has the lowest activation energy in agreement with the easiest removal of crystal water molecules.
2. The negative ΔS sign suggests a degradation via an abnormal pathway for those steps, and the degradation processes are undesirable. It is also evidence for a more ordered and organized activated complex. This can occur through the chemisorption of oxygen and other decomposition products. The more organized nature will refer to the activated state's bond polarization that takes place during electronic transitions.^[43]
3. The positive ΔH sign indicates the endothermic state of decomposition steps.
4. The positive ΔG sign points to the non-spontaneous nature of decomposition steps. Also, increasing the negative value of ΔS leads to a sequenced increase in ΔG values.^[44]

3.7 | Stoichiometry and formation constants of complexes

The stoichiometry of new complexes that developed in solution between FCAP and each metal salt (V (IV)O, Mn (II), Pd (II), and Zn (II)) was evaluated by continuous variations and molar ratio routes. The curves obtained from continuous variation and molar methods (cf. Figures 3 and S3) show maximum absorbance at mole fraction equal to 1 M:1 L in the molar ratio for Pd (II) and Zn (II) and 1 M:2 L for V (IV)O and Mn (II). Although the acceptable difference in complex composition is prepared in either solid state or solution, congruence gives an enhancement to the composition proposed for solid complexes.^[45] Also, the formation constant (K_f) of each complex was calculated from the continuous variation method (cf. Table 3). Accordingly, the order of stability of the complexes was proposed as follows: FCAPMn > FCAPVO > FCAPPd > FCAPZn complex. Furthermore, Gibbs free energy values were additionally obtained to indicate the spontaneous nature of complex formation.^[46] Based on the spectral and physical data of the complexes discussed above, it can be derived that through the deprotonated oxygen and the azomethine molecule, metal ions were attached to the Schiff base ligand, and the structure representation of the complexes was delineated in Scheme 1.

3.8 | pH stability range of complexes

The pH profile of the complexes displayed typical dissociation curves (cf. Figure 4), and the stability range is high up to pH = 4–9. A noticeable wide steady range of pHs reflects stability complexes than their free ligand. So, the different applications on such complexes over the pH = 4–9 range may happen without affection.

3.9 | DFT calculations

3.9.1 | Molecular DFT ligand FCAP calculation

The optimized FCAP structure is described in Figure 5 as the lowest energy configurations. The natural charges obtained from the natural bond orbital (NBO) analysis

TABLE 2 Plausible thermal degradation for the prepared FCAP metal as well as kinetic and thermodynamic parameters

Metal chelates	Temperature (°C)	Loss of fragment (%)		Loss of weight %		E* (KJmol ⁻¹)	A (S ⁻¹)	ΔH* (KJmol ⁻¹)	ΔG* (KJmol ⁻¹)	ΔS* (Jmol ⁻¹ K ⁻¹)
		Molecular formula	M. Wt.	Found	Calc.					
FCAPMn	35–120	2H ₂ O	36	4.93	(4.90)	157.80	1.85	157.15	174.99	–228.69
	122–180	2H ₂ O	36	4.86	(4.90)			156.54	191.91	–234.18
	182–280	C ₁₀ H ₉	129.18	17.54	(17.57)			155.88	210.79	–237.71
	282–370	C ₁₀ H ₉	129.18	17.52	(17.57)			155.09	233.52	–240.58
	372–460	C ₇ H ₅ NO	119.12	16.18	(16.20)			154.34	255.27	–242.61
	462–535	C ₇ H ₅ NO	119.12	16.16	(16.20)			153.65	275.47	–244.12
Residue	>540	MnO + 2 FeO	214.62	29.15	(29.19)					
FCAPPd	35–120	H ₂ O	18	3.53	(3.56)	148.80	1.39	148.15	166.17	–231.06
	122–280	CH ₃ COO + H ₂ O	77	15.21	(15.23)			147.13	195.16	–238.94
	282–450	C ₁₀ H ₉	129.18	25.22	(25.25)			145.76	235.03	–243.92
	452–610	C ₇ H ₅ NO	119.12	23.51	(23.56)			144.39	275.55	–247.01
Residue	>610	PdO + FeO	197.26	38.97	(39.01)					
FCAPVO	35–120	H ₂ O	18	2.57	(2.60)	159.30	0.094	158.65	178.42	–253.46
	122–280	C ₁₀ H ₉	184.8	26.68	(26.66)			157.63	210.16	–261.34
	282–391	C ₁₀ H ₉	184.8	26.61	(26.66)			156.50	246.02	–265.63
	393–465	C ₇ H ₅ NO	119.12	17.21	(17.18)			155.73	270.55	–267.64
	467–510	C ₇ H ₅ NO	119.12	17.19	(17.18)			155.23	286.64	–268.73
Residue	>510	VO + 2FeO	210.62	30.33	(30.38)					
FCAPZn	35–116	2H ₂ O	36	7.40	(7.41)	150.30	0.58	149.68	167.53	–238.01
	118–180	H ₂ O	18	3.75	(3.71)			149.06	185.37	–243.71
	182–295	NO ₃	62	12.80	(12.77)			148.32	207.25	–247.61
	297–450	C ₁₀ H ₉	129.18	26.56	(26.60)			147.20	240.95	–251.34
	452–612	C ₇ H ₅ NO	119.12	24.50	(24.53)			145.88	281.16	–254.3
Residue	>597	ZnO + FeO	153.23	31.52	(31.55)					

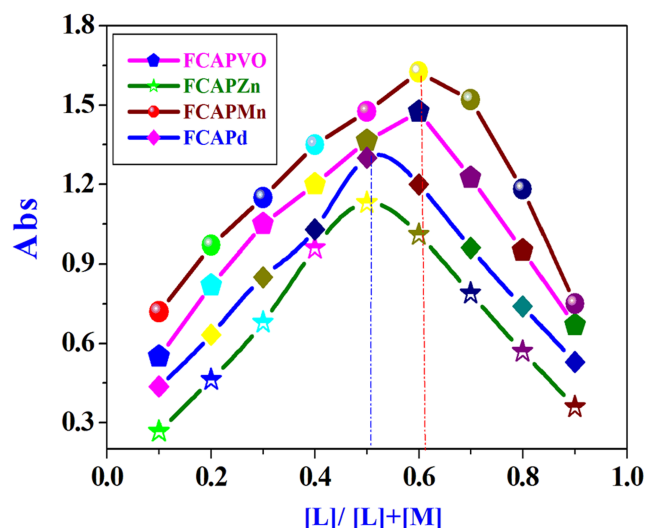


FIGURE 3 The curves of Job's method of synthesized FCAP complexes in DMF at $[M] = [FCAPM] = 10^{-3}$ M at 298 K

indicate that O9(−0.625) > N2(−0.581) and Fe(0.218) are the more negative active sites. Therefore, bidentate coordination is preferred by metal ions to O9 and N2, forming a stable five-membered ring.

3.9.2 | Molecular DFT complex FCAPVO calculation

The optimized structure of the complex FCAPVO is shown in Figure 6 as the lowest energy configurations. In a distorted square pyramidal geometry, where the atoms N2, O9, N54, and O56 deviate from the plane by -13.31° , the vanadium atom is five-coordinate (Table 4). V(+0.881), O56(−0.687), O9(−0.662), O31(−0.430), N54(−0.485), and N9(−0.483) are the natural charges computed from the NBO analysis on the coordinated atoms.

3.9.3 | Molecular DFT complex FCAPMn calculation

The optimized structure of the complex FCAPMn is presented in Figure 6 as the lowest energy configurations.

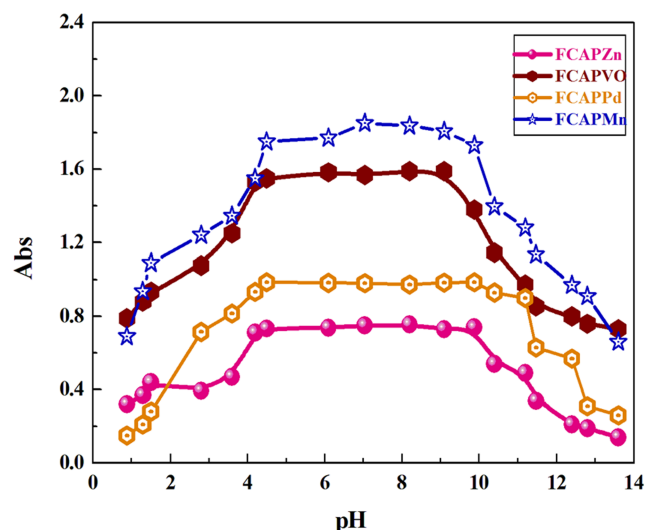


FIGURE 4 Impact of pH on FCAPZn, FCAPPd, FCAPMn, and FCAPV complexes at 25°C in aqueous media

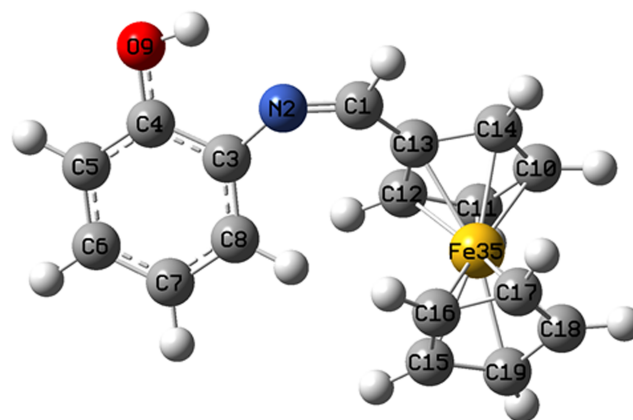


FIGURE 5 The optimized structure of FCAP by density function B3LYP/LANL2DZ

In a distorted octahedral geometry, the manganese atom is six-coordinate, where the atoms (N2, O9, N61, and O61), (O9, O36, O64, and O68) and (N2, O36, N61, and O68) are deviated by -10.23 , -7.750 , and -11.64 from the plane, respectively (Table 4). From the NBO analysis, the natural charges calculated on the coordinated atoms are Mn(+0.644), O9(−0.671), O64(−0.598), O68(−0.885), O61(−0.855), N61(−0.514), and N2(−0.478).

Complex	Type of complex	K_f	$\log K_f$	ΔG° (KJmol $^{-1}$)
FCAPMn	1:2	7.62×10^7	7.88	−44.97
FCAPZn	1:1	2.71×10^4	4.43	−25.29
FCAPPd	1:1	4.31×10^4	4.63	−26.44
FCAPVO	1:2	5.15×10^7	7.71	−43.99

TABLE 3 The formation and stability constants and Gibbs free energy $\Delta(G^\circ)$ values of the investigated FCAP metal chelates at 298 K

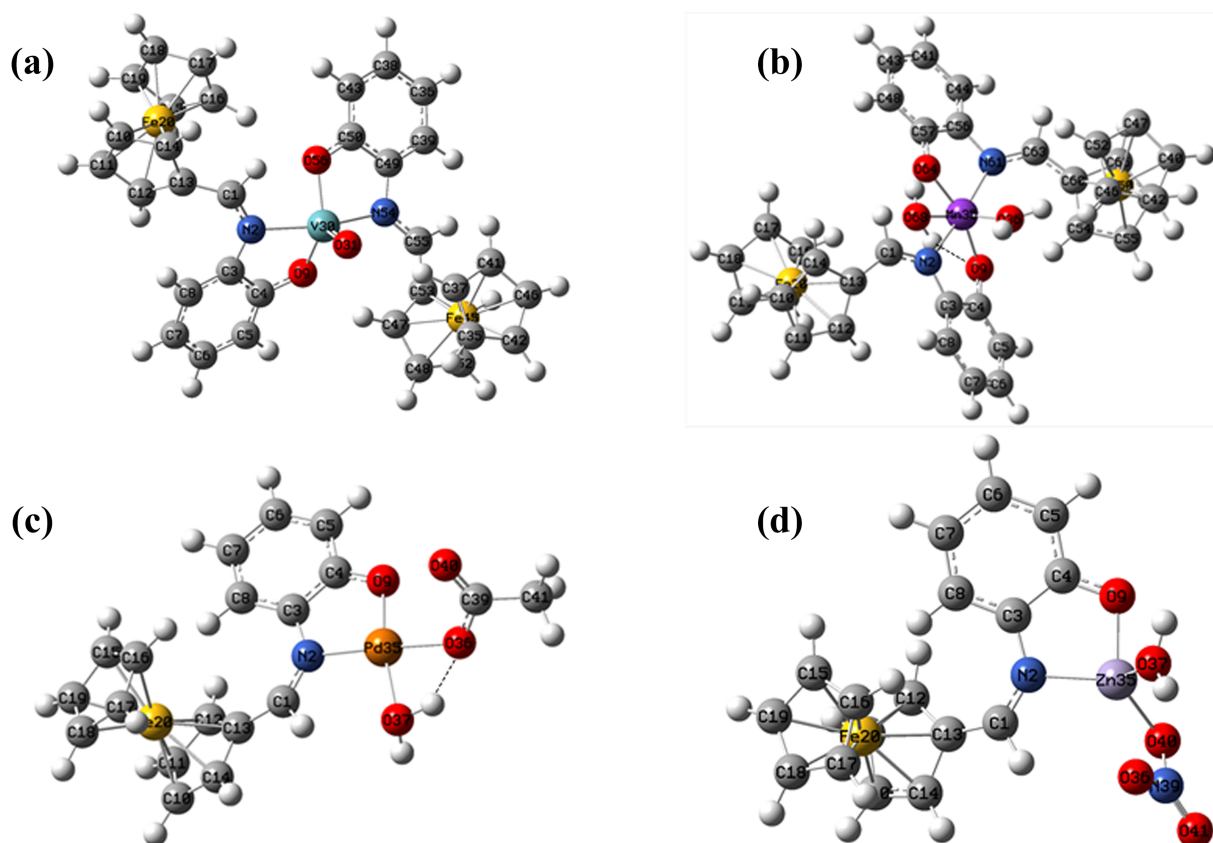


FIGURE 6 The optimized structure of (a) FACPVO, (b) FACPMn, (c) FACPPd, and (d) FCAPZn complexes using B3LYP/LANL2DZ

TABLE 4 Significant optimized bond angles ($^{\circ}$) and bond lengths (\AA) of the prepared FCAP metal chelates

Complex	Bond type	Bond length (\AA)	Angle type	Angle ($^{\circ}$)	Angle type	Angle ($^{\circ}$)
FACPVO	V=O31	1.610	O31-V-N2	100.9	O9-V-N2	79.55
	V-O9	1.905	O31-V-N54	100.4	O56-V-N54	80.90
	V-O56	1.913	O31-V-O9	115.9	O9-V-N54	92.01
	V-N2	2.133	O31-V-O56	117.4	O56-V-N2	88.45
	V-N54	2.144	N2-V-N54	158.6	O9-V-O56	126.6
			Fe20-V-Fe45	173.6	N2-O9-N54-O56	-13.31*
FACPMn	Mn-O9	1.919	O64-Mn-N61	83.91	O9-Mn-N2	80.68
	Mn-O54	1.872	O64-Mn-N2	89.35	O9-Mn-N61	106.2
	Mn-O36	1.980	O68-Mn-O9	76.29	O36-Mn-O9	95.23
	Mn-N2	2.064	O68-Mn-O64	89.16	O36-Mn-O64	99.54
	Mn-N61	2.031	O68-Mn-N2	94.96	O36-Mn-N2	85.48
	Mn-O68	2.119	O68-Mn-N61	86.34	O36-Mn-N61	94.26
			N2-Mn-N61	173.1	O9-Mn-O61	161.5
			O36-Mn-O68	171.3	N2-O9-N61-O64	-10.23*
			Fe20-Mn-Fe50	160.2	O9-O36-O64-O68	-7.750*
FACPPd					N2-O36-N61-O68	-11.64*
	Pd-O9	1.991	N2-Pd-O9	83.13	O36-Pd-O37	73.14
	Pd-O36	2.050	N2-Pd-O37	105.1	O9-Pd-O36	98.53
	Pd-N2	2.057	N2-Pd-O36	177.2	O9-Pd-O37	171.0
	Pd-O37	2.181			O9 N2-O37-O36	1.114*

(Continues)

TABLE 4 (Continued)

Complex	Bond type	Bond length (Å)	Angle type	Angle (°)	Angle type	Angle (°)
FACPZn	Zn-O9	1.965	N2-Zn-O9	84.66	O37-Zn-O40	109.5
	Zn-N2	2.081	N2-Zn-O40	116.0	O9-Zn-O37	90.72
			N2-Zn-O37	126.5	O9-Zn-O40	125.8

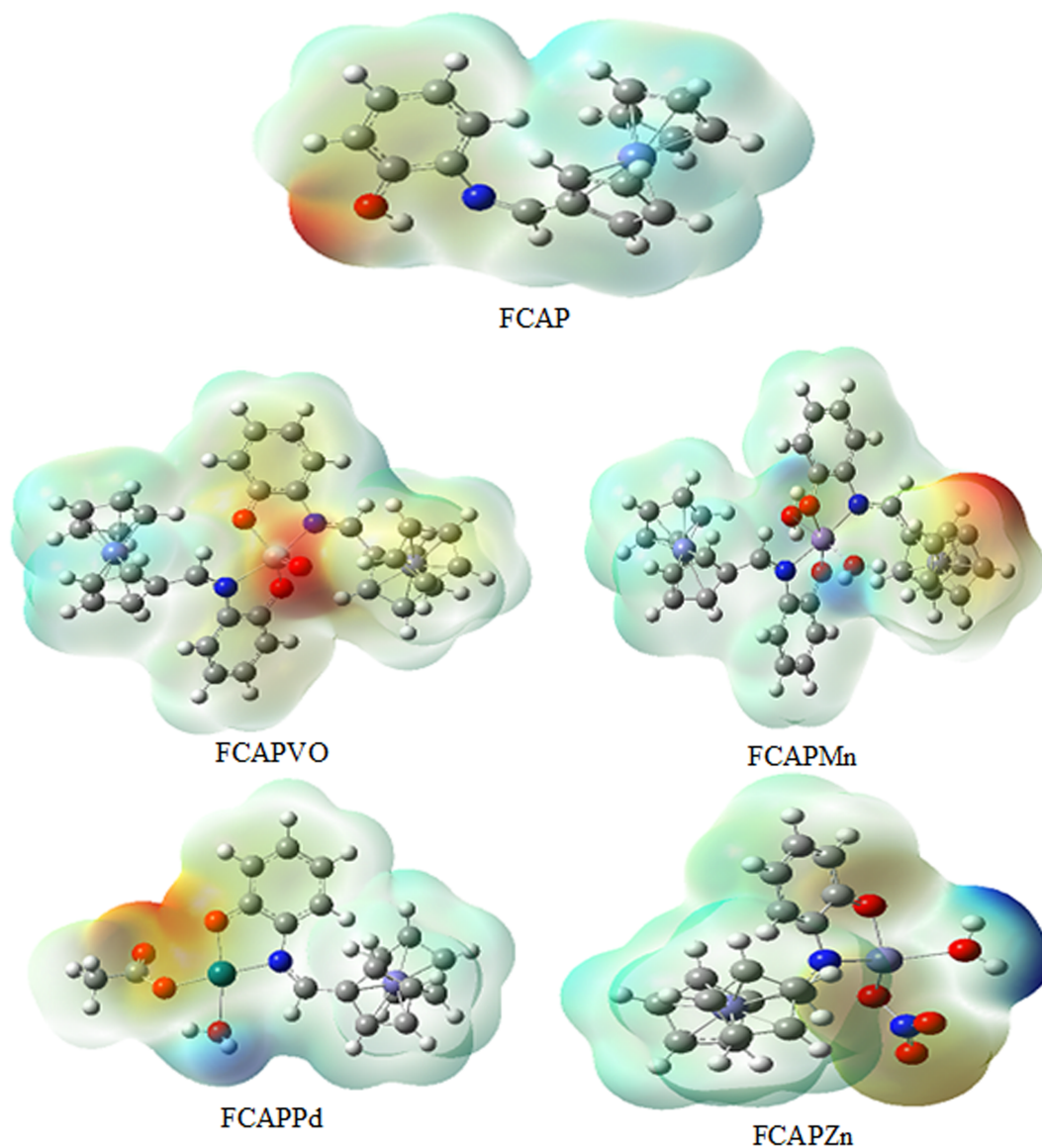


FIGURE 7 Molecular electrostatic potential (MEP) surface of FCAP and complexes FCAPVO, FCAPMn, FCAPPd, and FCAPZn

TABLE 5 Estimated energies of FCAP ligand and its metal chelates at B3LYP/LANL2DZ

	E (a.u.)	HOMO (eV)	LUMO (eV)	E _g (eV)	Dipole moment (Debye)
FCAP	−910.10	−5.6885	−1.8683	3.8202	4.7194
FCAPVO	−1198.10	−8.5940	−5.3373	3.2567	11.950
FCAPMn	−2075.16	−3.6915	−3.0722	0.6193	11.8283
FCAPPd	−1341.17	−5.5152	−2.5265	2.9887	9.6167
FCAPZn	−1331.90	−5.4883	−2.3312	3.1571	6.7733

Note. E is the total energy (a.u.). $E_g = E_{\text{LUMO}} - E_{\text{HOMO}}$.

Abbreviations: HOMO, highest occupied molecular orbital; LUMO, lowest unoccupied molecular orbital.

3.9.4 | Molecular DFT complex FCAPPd calculation

The optimized structure of the FCAPPd complex is shown in Figure 6 as the lowest energy configurations. In a distorted square planar geometry, the palladium atom is four-coordinate, where the atoms O9, N2, O37, and O36 are deviated by 1.114° from the plane (Table 4). From the NBO analysis, the natural charges computed on the coordinated atoms are Pd(+0.727), O9(−0.616), N2(−0.478), O36(−0.797), and O37(−0.937).

3.9.5 | Molecular DFT complex FCAPZn calculation

The optimized structure of the complex FCAPZn is shown in Figure 6 as the lowest energy configurations. In

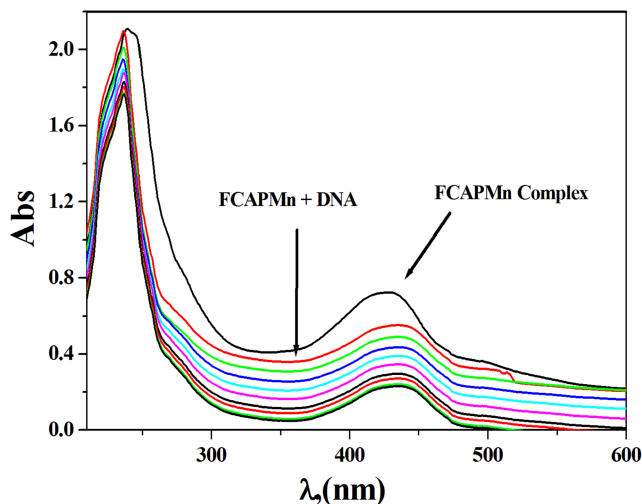


FIGURE 8 FCAPMn complex absorption spectra at 0.01 mol dm^{-3} Tris buffer (pH 7.5, 298 K) after addition of ctDNA in absence (lower) and ctDNA presence (top) at $[\text{FCAPMn}] = 10^{-3} \text{ mol dm}^{-3}$ and $[\text{ctDNA}]$ (0–50) μM

a distorted tetrahedral geometry, the zinc atom is four-coordinate. From the NBO analysis, the natural charges computed on the coordinated atoms are Zn(+1.398), O9(−0.876), N2(−0.641), O40(−0.608), and O37(−1.001).

The surface of the molecular electrostatic potential (MEP) to locate the positive (blue color) and negative (red color, excess electrons or loosely bound) charged electrostatic potential in the molecule is shown in Figure 7. The computed total energy, the lowest unoccupied molecular orbital (LUMO) energies, the highest occupied molecular orbital (HOMO) energies, and the dipole moment for the FCAP ferrocenyl imine ligand and its metal chelates were calculated (Figure S4 and Table 5). The complexes' more negative total energy values than those of free FCAP ligand suggest that they are more stable than free FCAP ligand.

3.10 | DNA binding studies for the investigated complexes

3.10.1 | Absorbance spectral studies

UV–vis absorbance is the most valuable tool to evaluate the mode of the interaction and the binding ability of interesting small molecules and their corresponding M-complexes with ctDNA. The latter interaction with complexes is derived either from hypochromism or bathochromism, as the binding usually includes a strong interaction between the DNA nitrogen bases and the ligand (e.g., aromatic moiety). Furthermore, the metal chelate could bind to the double-stranded DNA within different interaction modes depending on its charge, structure, and nature of the molecule.^[16] Generally, shifts and/or changes in the absorbance characteristic bands of the M-chelate could be observed, when it interacts with DNA.^[18,30] The strength of such interaction could be correlated with the magnitude of such shift and/or change

TABLE 6 Spectral parameters for the interaction of the investigated FCAP metal chelates with DNA

Complex	λ_{max} free (nm)	λ_{max} bound (nm)	Δn	Chromism (%)	Type of chromism	Binding constant 10^4 (K_b)	ΔG^* (KJmol^{-1})
FCAPMn	426	435	9	25.00	Hypo	3.26	−25.75
	238	236	2	4.76	Hypo		
FCAPPd	420	423	3	22.47	Hypo	6.80	−27.60
	320	318	2	19.05	Hypo		
	247	248	1	8.85	Hypo		
	239	237	2	6.60	Hypo		
FCAPVO	426	435	9	32.22	Hypo	2.20	−24.80
	239	238	1	4.27	Hypo		
FCAPZn	424	433	9	29.91	Hypo	5.70	−27.10
	238	236	2	3.32	Hypo		

in the absorbance. For the covalent binding, a labile coordinated ligand in the M-complex could be replaced by the nitrogen base of DNA such as guanine N7 (e.g., solvent molecules).^[47] On the other hand, all the electrostatic interaction, the intercalative action, and groove (surface) binding of the M-chelating complexes outside the DNA helix, along the minor or major groove, could be considered as non-covalent interactions.^[27] Within the intercalative interaction mode, the π^* orbital of the intercalated ligand in its M-complex could couple with the π orbital of the DNA base pairs, causing a decrease in the $\pi \rightarrow \pi^*$ transition energy and resulting in hypochromism.^[18,20]

Accordingly, the binding capability of FCAPZn, FCAPPd, FCAPMn, and FCAPVO complexes with ctDNA was investigated by measuring their electronic spectral variation during the DNA interaction (Figures 8 and S5). The representative spectra show that the absorption bands of each investigated complex were affected upon increasing amounts of DNA. This points to a hypochromic effect derived from the interaction of the investigated complexes with ctDNA. On the other hand, the hyperchromic shift suggests electrostatic interaction between negatively charged DNA and electropositive molecules. The intrinsic binding constants (K_b) calculated from Figure S4 for the current M-complexes, as shown in Table 6, are in the following order: FCAPZn > FCAPPd > FCAPMn > FCAPVO complex.

3.10.2 | Viscosity measurements

Viscosity measurements were progressed to investigate the binding mode between the synthesized complexes

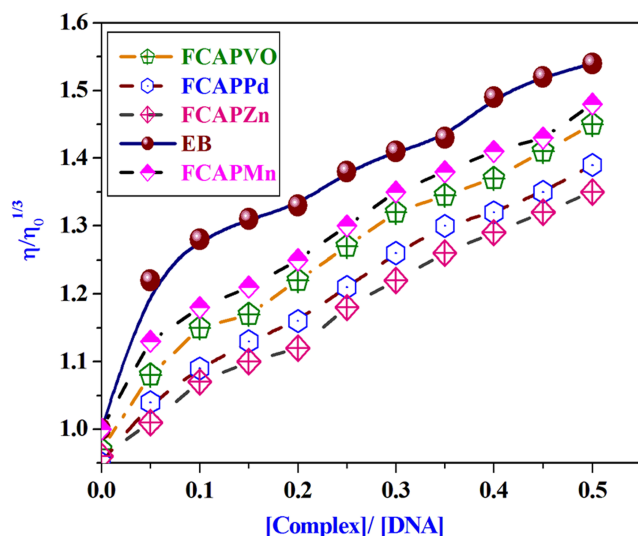


FIGURE 9 The effect of increasing the amount of the synthesized complexes on the relative viscosities of ctDNA at [DNA] = 0.5 mM at 298 K

and DNA in solution. Hydrodynamic measurements are sensitive to the change of the DNA molecule nature, that is, the length and bending, which may take place as a result of its different binding modes with the complex compounds.

From Figure 9, the plotting of the relative viscosity $(\eta/\eta_0)^{1/3}$ against $r = \text{the ratio of } [\text{complex}]/[\text{DNA}]$ (form 0–0.5 mM) assigned a significant enhancement in the relative viscosity of DNA with improving the M-complex concentration. Each probe is similar to that positive intercalator reference EB.^[48] Therefore, the overall increase in DNA length and viscosity may be due to the intercalation between the DNA base pairs and the M-complexes. Collectively, the viscosity results and the molecular docking studies are in good agreement and suggest base pair intercalation mode.

3.10.3 | Gel electrophoresis for the interaction between the complexes investigated and DNA

Gel electrophoresis is an important technique for examining the nature of the binding of compounds with nucleic acids of DNA. Comparing the DNA gels before and after its mixing with the investigated current complexes, it could be observed that the staining intensity of

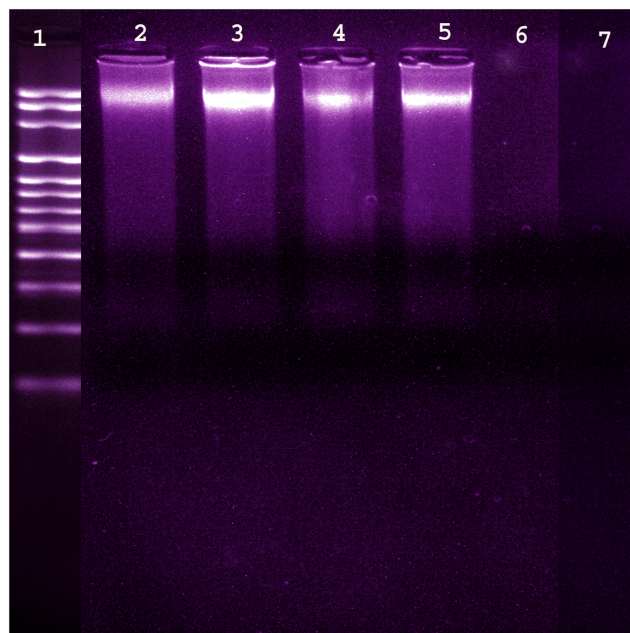


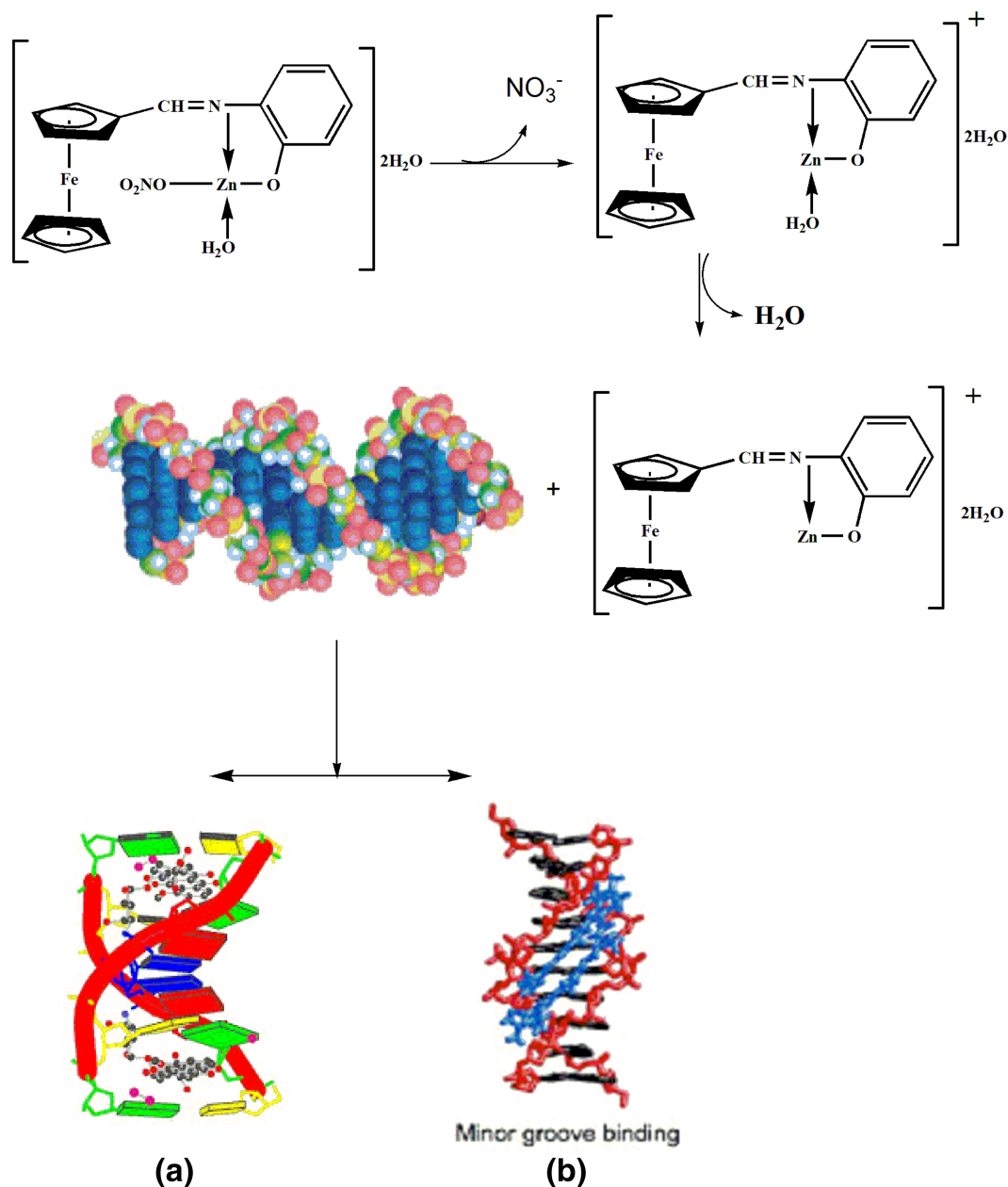
FIGURE 10 The interaction of the investigated complexes with ctDNA was studied by agarose gel electrophoresis. Lane 1: DNA ladder, Lane 2: ctDNA + FCAPZn, Lane 3: ctDNA + FCAPVO, Lane 4: ctDNA + FCAPPd, Lane 5: ctDNA + FCAPMn, and Lane 6: FCAPPd complex and FCAPMn complex

the gel was slightly reduced for the mixed one with the titled metal chelates. Particularly, with the FCAPPd complex, the DNA staining intensity reduced, referring to the strong DNA interaction with this complex, as shown in Figure 10. Consequently, the effect of such current metal imine chelates on the growth of the pathogenic organism could be attributable to their genomic interaction.^[18,30]

3.10.4 | The proposed mechanism for the DNA interaction

Taking together the spectral investigations and hydrodynamic obtained between the current reagents (FCAPZn,

FCAPPd, FCAPMn, and FCAPVO) and DNA, alternative binding interaction modes could be proposed. The investigated complexes interact with DNA most likely through an electrostatic or hydrophobic interaction mode. For example, the replacement of the FCAPZn complex acetate group by water molecules by DNA interaction results in a positive charge on the complex. An electrostatic binding (see Scheme 2) was then proposed in addition to intercalation and substitution in the case of that complex. The FCAPMn complex has replaceable coordinated H₂O molecules. Removal of these coordinated water molecules will lead to a flat part in the middle of the FCAPMn complex. Therefore, the proposed interaction of the FCAPMn complex, for example,



SCHEME 2 Suggested mechanism for FCAPZn complex interaction with DNA through (a) electrostatic and (b) minor groove binding

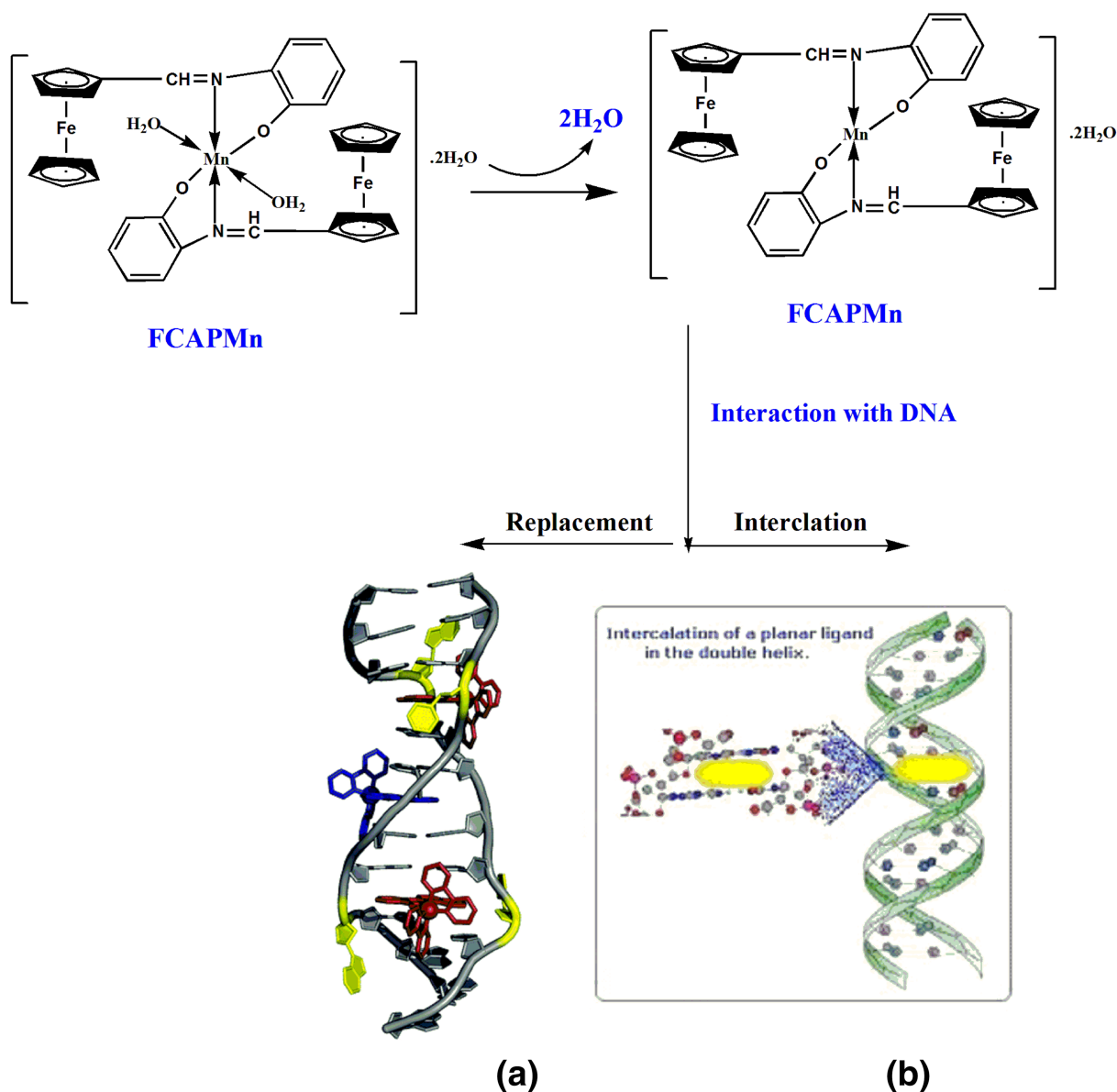
with DNA, could be via intercalation or replacement as presented in Scheme 3.^[49]

3.11 | Antimicrobial activity of the newly synthesized compounds

The interesting DNA binding studies of the newly synthesized complexes encouraged us to further investigate their corresponding antimicrobial activities. Mounting reports have shown that transition metal complexes possess good antimicrobial activity. Therefore, the antimicrobial activity of FCAPZn, FCAPPd, FCAPMn, and FCAPVO complexes and their uncoordinated ligand FCAP was tested within the well diffusion method^[4,5,19]

against *M. luteus* G (+) bacteria and two G (–) bacteria, namely, *S. marcescens* and *E. coli* as well as *A. flavus*, *G. candidum*, and *F. oxysporum* fungal strains. The results are shown in Table 7, and Figure 11 is compared with the standard antibiotics, ofloxacin (for bacteria), and amphotericin B (for fungi). The clear zones around the discs are the inhibition zones, measured in millimeter, and their respective percent activity index was also tabulated (Table S2).

As expected, the free ligand FCAP exhibited lower antimicrobial activity than their corresponding complexes. The antimicrobial activity of the M (II) complexes compared with their respective uncoordinated ligand might be interpreted employing Overtone's and Tweedy's concept.^[4,5,19,50]



SCHEME 3 Suggested mechanism for FCAPMn complex interaction with DNA through (a) intercalation binding and (b) replacement

TABLE 7 Antimicrobial bioassay data of the investigated compounds against selected strains of bacteria and fungi

Compounds	±SD inhibition zone (mm)											
	Serratia marcescens (-ve)		Escherichia coli (-ve)		Micrococcus luteus (+ve)		Aspergillus flavus		Geotrichum candidum		Fusarium oxysporum	
Conc. (µg/ml)	10	20	10	20	10	20	10	20	10	20	10	20
FCAP	4.5 ± 0.10	7.6 ± 0.06	3.45 ± 0.1	5.8 ± 0.05	6.1 ± 0.08	9.8 ± 0.14	3.1 ± 0.10	6.7 ± 0.10	7.2 ± 0.07	12.1 ± 0.20	5.2 ± 0.10	8.3 ± 0.14
FCAPVO	12.8 ± 0.11	26.8 ± 0.10	10.7 ± 0.05	20.7 ± 0.13	17.6 ± 0.10	38.1 ± 0.23	10.1 ± 0.03	17.8 ± 0.31	18 ± 0.21	35.2 ± 0.12	11.5 ± 0.17	23.2 ± 0.14
FCAPPd	14.20 ± 0.08	30.5 ± 0.32	13.1 ± 0.10	24.1 ± 0.08	21.2 ± 0.11	41.5 ± 0.10	12.5 ± 0.11	21.5 ± 0.21	20.7 ± 0.23	38.5 ± 0.15	14.1 ± 0.10	26.50 ± 0.02
FCAPMn	11.50 ± 0.20	25.2 ± 0.17	9.85 ± 0.22	19.1 ± 0.11	15.90 ± 0.10	37.2 ± 0.16	9.55 ± 0.10	16.1 ± 0.31	17.3 ± 0.31	33.9 ± 0.17	10.2 ± 0.15	21.4 ± 0.13
FCAPZn	13.50 ± 0.12	28.7 ± 0.11	11.9 ± 0.07	22.90 ± 0.12	19.3 ± 0.15	40.25 ± 0.03	11.3 ± 0.05	19.6 ± 0.21	19.55 ± 0.25	36.7 ± 0.17	12.80 ± 0.17	24.90 ± 0.12
Ofloxacin	15.70 ± 0.11	32.20 ± 0.20	14.5 ± 0.05	26.5 ± 0.15	23.80 ± 0.13	44.5 ± 0.11						
Fluconazol							13.60 ± 0.20	23.7 ± 0.09	22.5 ± 0.06	40.3 ± 0.07	15.50 ± 0.11	28.2 ± 0.25

The microdilution method (MIC) results are in good agreement with the well diffusion assay, and data are given in Table S3 and presented in Figure 12. It is clear from the data that the FCAPPd complex (MIC: 2.75, 3.25, and 2.25 µM) has shown the best bacterial activity against *S. marcescens*, *E. coli*, and *M. luteus* in comparison with other complexes. Upon complexation, the lipophilicity of the transition metal ions is increased due to the delocalization of the π -electrons among the complex sphere. This in turn improves the diffusion through the cell membrane. Although chelation plays a significant role in the determination of the antimicrobial behavior of the complexes, other factors may also enhance and control the antimicrobial activity of metal complexes compared with the free ligand. These include size, dipole moment, solubility, complexation sites, the redox potential of metal ion, solubility, the bond length between the ligand and metal, complexes geometry, steric, pharmacokinetic, concentration, and hydrophobicity.^[30,51] In addition, the variation in the behavior of the metal complexes against different microbes can also depend on the preferential difference in the microbes' cell wall permeability. On comparing the antimicrobial activity with other related ferrocenyl Schiff base complexes in literature,^[52] we found that our compounds show potent activity than these compounds against *E. coli* bacteria considering variation of the concentration of the tested compounds in the investigation.

The anticancer activity of FCAP, FCAPZn, FCAPPd, FCAPMn, and FCAPVO samples was examined against three different human cancer cells, namely, HCT-116, MCF-7, and HepG-2 cells. Doxorubicin was used as the standard, and the corresponding IC₅₀ values were determined and recorded in Table S4. In general, the cancer cells' (MCF-7, HepG-2, and HCT-116) growth decreased in a concentration-dependent manner upon treatment with tested compounds; however, the antiproliferative activity was less than vinblastine. Furthermore, the investigated FCAP metal chelates were more cytotoxic than the corresponding free FCAP ligand. This might be due to the presence of the metal redox-active center.^[53,54] Moreover, the cytotoxicity was more pronounced against MCF-7 compared with the other cancer cells (HepG-2 and HCT-116). Interestingly, the FCAPPd complex exhibited superior cytotoxicity against all the three applicable cell lines compared with other complexes and the free Schiff base ligands (cf. Figure 13). These results were in excellent agreement with that obtained from the antimicrobial screening. On comparing the anticancer activity with other related ferrocenyl Schiff base complexes in literature,^[52] we found that our compounds show potent activity than these compounds against breast tumor cells.

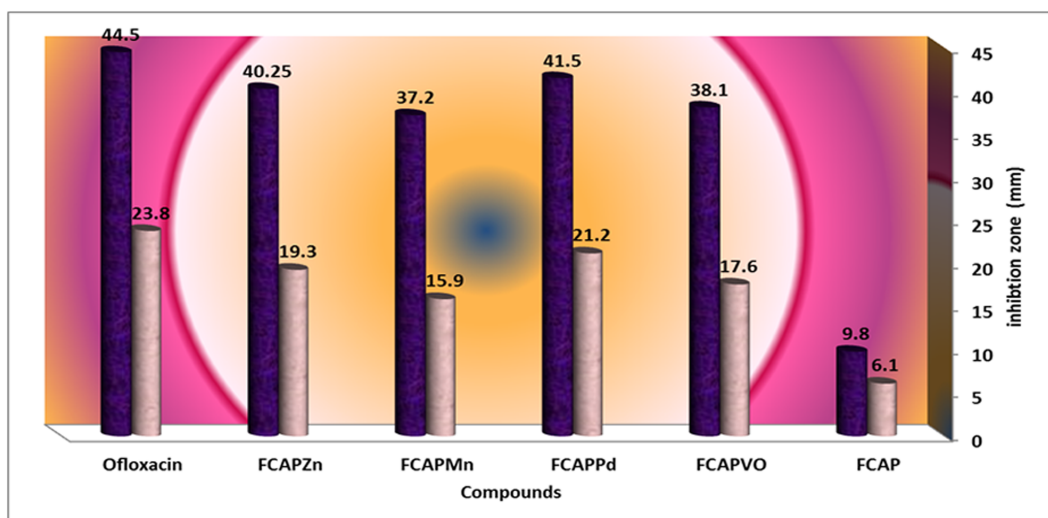


FIGURE 11 Histogram indicating antibacterial comparable activities of the prepared FCAP ligand and its FCAPZn, FCAPPd, FCAPMn, and FCAPV complexes against *Micrococcus luteus* bacteria

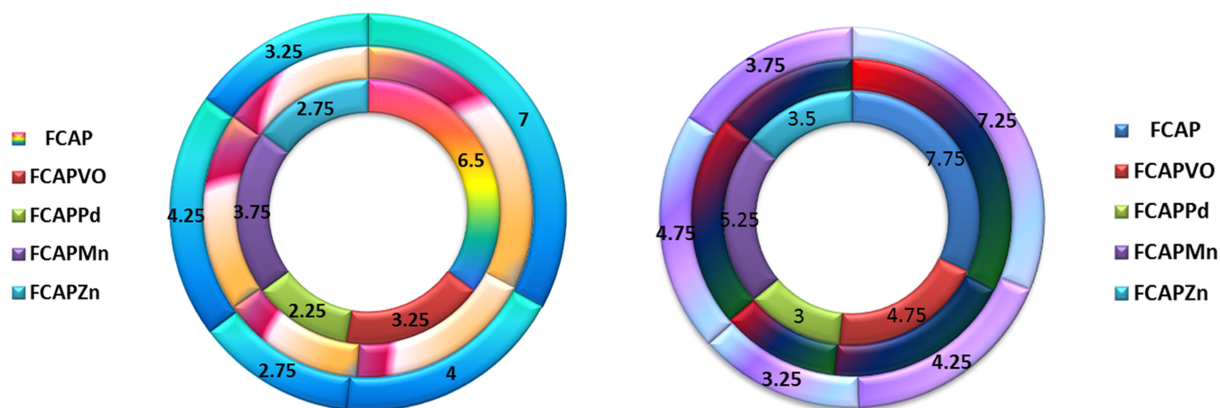


FIGURE 12 Histogram showing minimum inhibitory concentration for the investigated compounds against the investigated bacteria and fungi

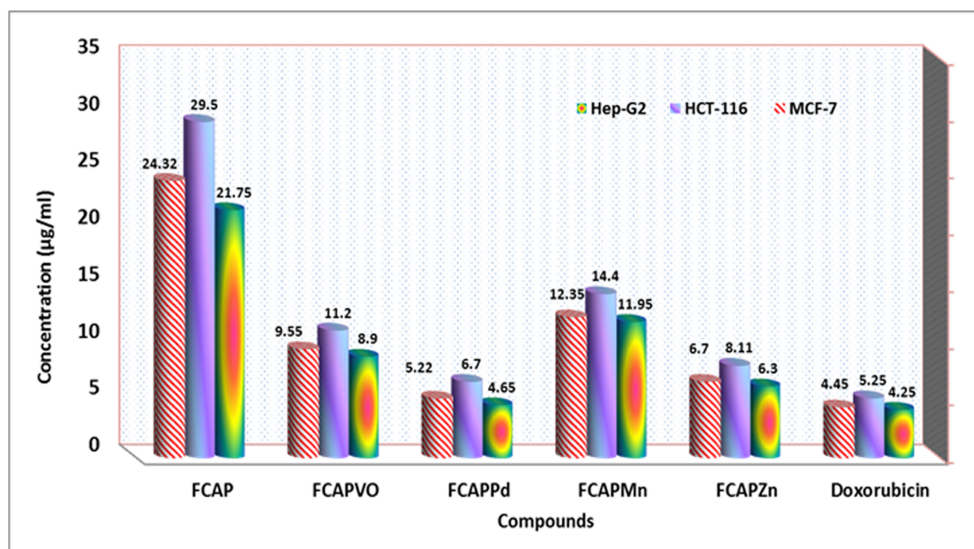


FIGURE 13 IC_{50} values against human colon carcinoma cells (HCT-116 cell line), breast carcinoma cells (MCF-7 cell line), and hepatic cellular carcinoma cells (HepG-2 cell line) of the FCAP mine ligand and its complexes

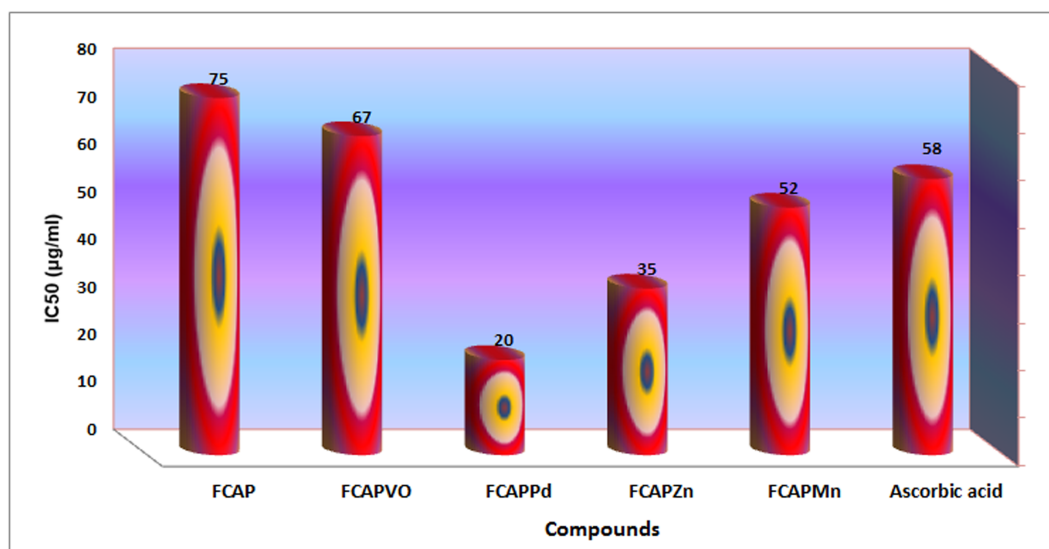


FIGURE 14 Trends in the inhibition of DPPH[•] radical by the FCAP ferrocenyl FCAP imine ligand and its metal chelates

TABLE 8 The docking interaction data calculations of FCAP, FCAPMn, FCAPPd, FCAPZn, and FCAPVO with the active site of the receptor of breast cancer oxidoreductase (PDB ID: 3HB5)

	Receptor	Interaction	Distance (Å)	E (kcal/mol)
FCAP				
N 2	NZ LYS 248	H-acceptor	2.83 (1.85)	−13.1
FCAPPd				
N 2	OE1 GLU 100	H-donor	3.12 (2.17)	−10.5
N 2	OE2 GLU 100	H-donor	3.14 (2.24)	−7.9
O 38	OE1 GLU 100	H-donor	2.91 (1.93)	−12.8
O 38	OD1 ASP 208	H-donor	2.95 (2.00)	−17.4
O 38	OE1 GLU 100	Ionic	2.91	−5.1
O 38	OD1 ASP 208	Ionic	2.95	−4.8
FCAPZn				
N 2	OE1 GLU 100	H-donor	3.42 (2.49)	−2.8
N 2	OE2 GLU 100	H-donor	3.19 (2.28)	−6.3
O 38	OE1 GLU 100	H-donor	2.71 (1.82)	−16.3
O 38	OD1 ASP 208	H-donor	2.75 (1.89)	−17.0
FE 21	OG1 THR 211	Metal	2.58	−0.9
O 38	OE1 GLU 100	Ionic	2.71	−6.7
O 38	OD1 ASP 208	Ionic	2.75	−6.4
FCAPMn				
O 36	OE1 GLU 235	H-donor	2.83 (1.92)	−22.3
FE 20	OE1 GLU 235	Metal	2.45	−3.3
N 2	OE1 GLU 235	Ionic	3.20	−3.3
O 36	OE1 GLU 235	Ionic	2.83	−5.7
FCAPVO				
N 2	OE1 GLU 100	H-donor	2.85 (1.92)	−6.3
O 32	OD1 ASP 208	H-donor	2.83 (1.91)	−7.4
FE 21	OE1 GLU 100	Metal	2.72	−0.9
FE 21	OE2 GLU 100	Metal	2.12	−5.4

Note. The lengths of H-bonds are in brackets.

3.12 | Antioxidant activity of the prepared compounds via DPPH assay

Collectively, the DNA binding, antimicrobial, and anti-cancer studies point to a potential activity of the newly synthesized compounds. These encourage us to further investigate their corresponding redox properties, which may also take part in their interesting activities.

The antioxidant potential of the novel synthesized complexes was further evaluated via the DPPH assay. The assay relies on the decolorization (at 517 nm) of the 1,1-diphenyl-2-picryl-hydrazine radical violet color upon the reaction of DPPH with free radical scavengers (i.e., antioxidants).^[55,56] The numbers of scavenged electrons were stoichiometric to the reaction. Ascorbic acid was used as a (+) control. The (−) control sample consists

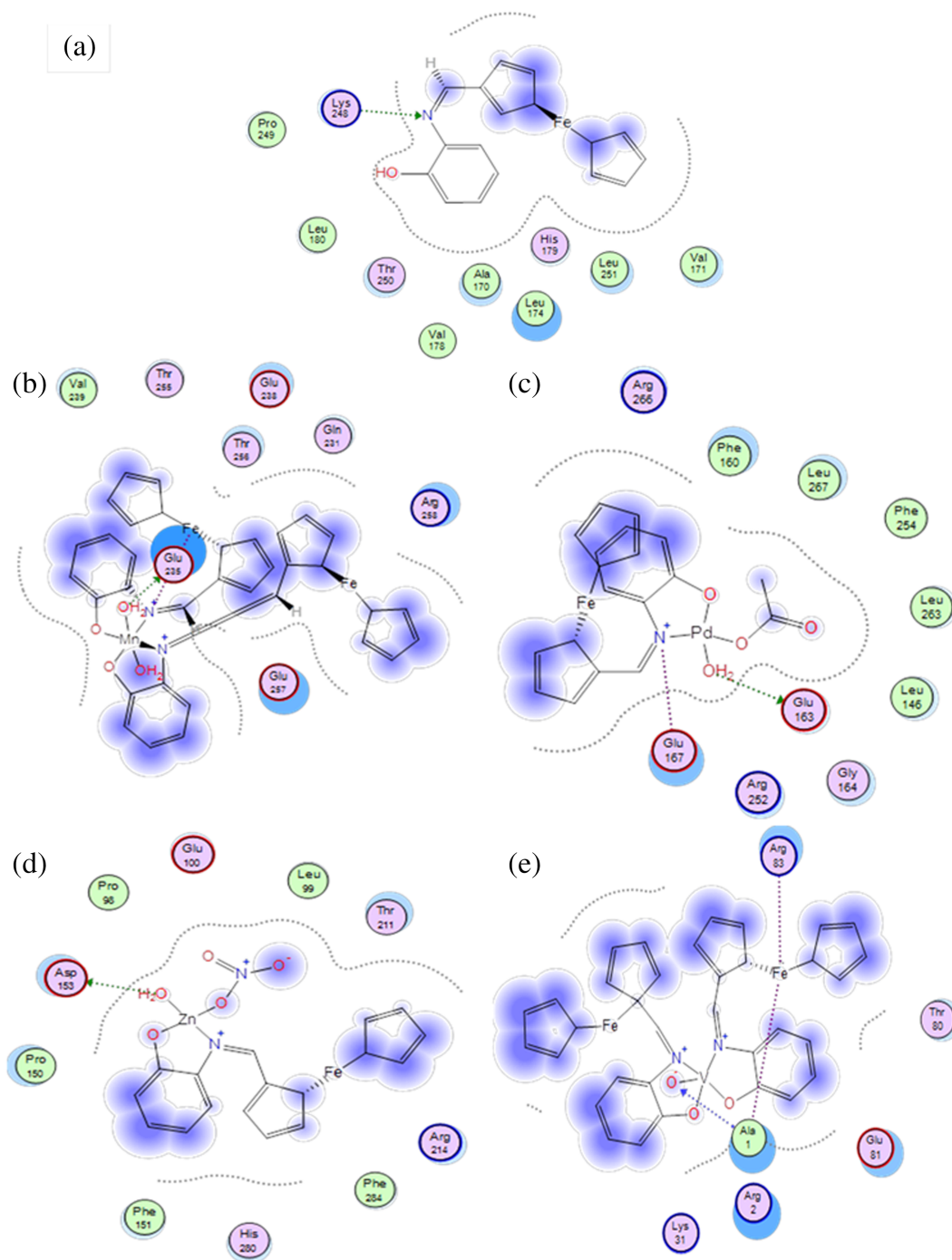


FIGURE 15 2D plot of the interaction between FCAP (a) and its complexes: FCAPPd (b), FCAPZn (c), (FCAP)2Mn (d), and FCAPVO (e) with the active site of the receptor of breast cancer (PDB ID: 3hb3). With dotted curves, hydrophobic interactions with amino acid residues are shown

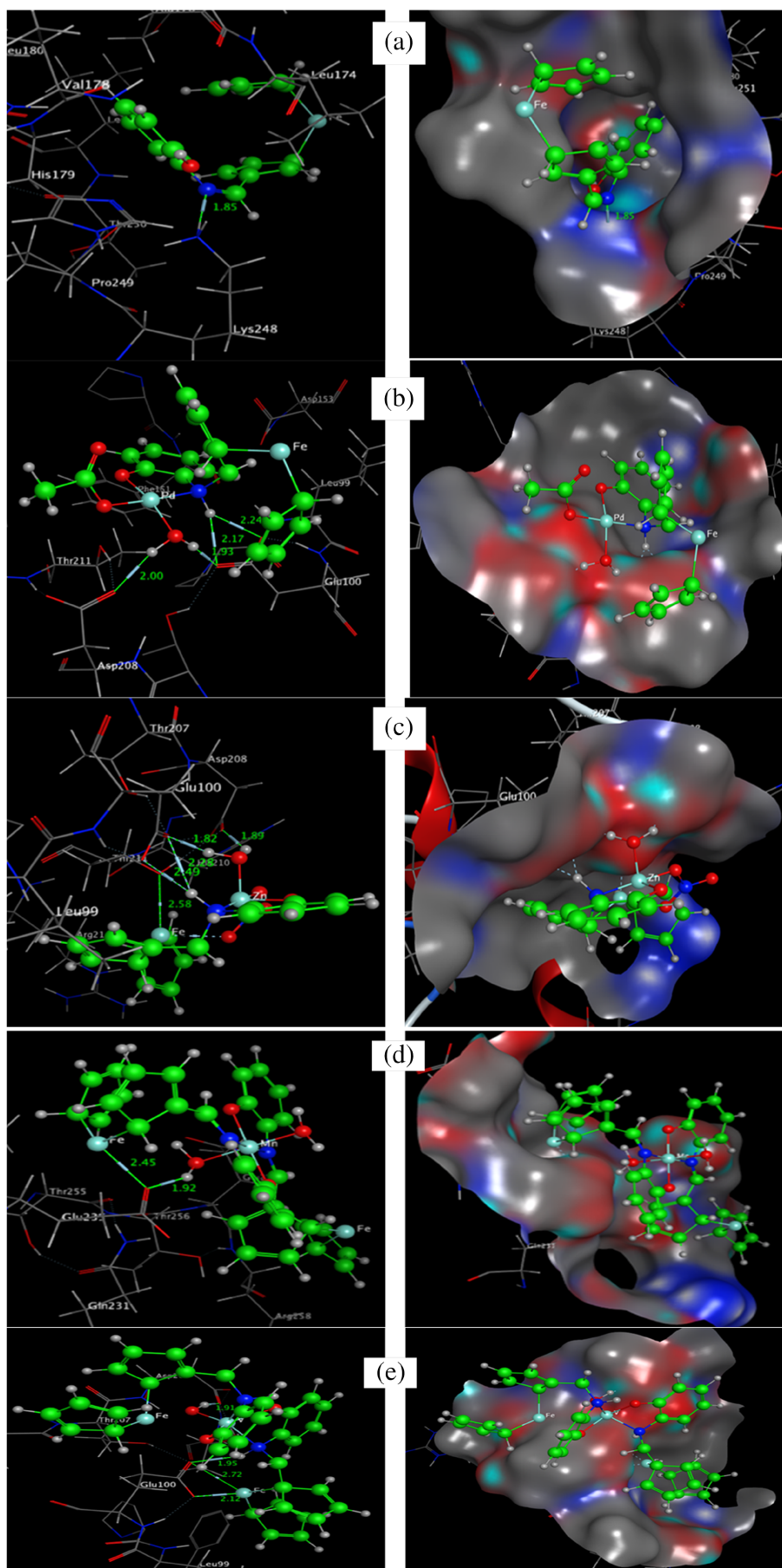


FIGURE 16 Molecular docking simulation studies of the interaction between FCAP (a) and its complexes: FCAPPd (b), FCAPZn (c), FCAPMn (d), and FCAPVO (e) with the active site of the receptor of breast cancer (PDB ID: 3hb3). The compound's docked conformation is shown in the ball and stick representation

of a methanolic solution of DPPH, whereas the blank sample is only methanol. The scavenging activity percentage of the investigated complexes (%) demonstrated moderate free radical-scavenging activity compared with ascorbic acid, as depicted in Figure 14.

3.13 | Molecular docking studies

Docking studies are regarded as a very efficient tool that can be used to assess the Schiff base ligand's multireceptor interaction to design the resistance of drug against various effects that occur in our bodies.^[57] The structure of the FCAP ligand and its VO^{2+} , Mn^{2+} , Zn^{2+} , and Pd^{2+} complexes were created in PDB file format from the output of Gaussian09 software. The crystal structures of the receptor of breast cancer (PDB ID: 3HB5) were downloaded from the protein data bank (<http://www.rcsb.org/pdb>). The molecular docking studies were performed using MOA2014 software, to find the possible binding modes of the most active site of the receptor of breast cancer oxidoreductase (PDB ID: 3HB5) (Table 8 and Figures 15 and 16). From the findings, it was shown that the ligand's main interaction force was H-acceptor, whereas some binding interaction also occurred in complexes alongside the ligand's main interaction, such as H-donor and ionic. The more negative the energy values, the more stable (stronger interaction). Thus, the order of binding of the prepared compounds towards the receptor is as follows: $\text{FCAPPd} > \text{FCAPZn} > \text{FCAPVO} > \text{FCAPMn} > \text{FCAP}$ compound. The obtained data are correlated with anticancer data against the breast cancer cell line and found to be in good agreement.

4 | CONCLUSION

Herein, we report the synthesis of ferrocene azomethine ligand (FCAP) and a series of its V (IV)O, Mn (II), Zn (II), and Pd (II) transition metal ions. Accordingly, different M^{2+} Schiff base complexes (FCAPZn, FCAPPd, FCAPMn, and FCAPVO) were synthesized in good yields (up to 85%) via the reaction with the corresponding metal. The respective chemical structures of all the synthesized compounds (FCAP, FCAPZn, FCAPPd, FCAPMn, and FCAPVO) were in excellent agreement with the obtained analytical data (NMR, IR, UV-vis, EA and TGA analyses, conductance measurements, and magnetic susceptibility). The data of elemental analysis confirmed that the FCAP ligand reacted with metal ions in 1:1 M ratio in the case of Zn (II) and Pd (II) and 1:2 M ratio for V (IV)O and Mn (II). IR spectra demonstrated that through deprotonated phenolic and azomethine

groups, ligand behaved as a bidentate ligand and was bound to metal ions. Correlation of all physicochemical properties for the prepared complexes with DFT calculations confirms the suggested structure of the prepared complexes. UV-vis absorption spectroscopy and hydrodynamic and gel electrophoresis measurements were performed to detect the interaction and binding mode of the newly synthesized complexes with DNA. Collectively, the results show that the absorption bands, as well as DNA length and viscosity, were affected. These indicate that the interaction of the complexes with DNA could be via intercalation or replacement, which was further supported by molecular docking studies. The antimicrobial activity of FCAPZn, FCAPPd, FCAPMn, and FCAPVO complexes and their free ligand FCAP was evaluated against *A. flavus*, *G. candidum*, and *F. oxysporum* fungal strains as well as *M. luteus* Gram-positive bacteria and two Gram-negative bacteria, namely, *S. marcescens* and *E. coli*. Furthermore, the antiproliferative activity of the investigated compounds and their free ligand FCAP was also evaluated against different cancer cells such as HCT-116, MCF-7, and HepG-2 cells. In general, the M^{2+} complexes exhibited better antimicrobial and anticancer activities than FCAP ligand, which might be due to the presence of the metal redox-active center. Moreover, the FCAPPd complex was the most active and inhibited the multiplication of the bacterial and fungal strains as well as the tested cancer cells. Additionally, the redox properties of the synthesized complexes were also evaluated via the DPPH assay. The tested compounds showed moderate-good antioxidant activities, particularly against the superoxide anion radicals, compared with ascorbic acid.

CONFLICT OF INTEREST

All authors agreed to state not any conflict of interest regarding any content or publication of this work in the form of a manuscript.

AUTHOR CONTRIBUTIONS

Enas Aljohani: Funding acquisition; investigation; methodology; software. **Mohamed Shehata:** Formal analysis; software; supervision; validation. **Fatmah Alkhatib:** Funding acquisition; methodology; resources. **Seraj Alzahrani:** Data curation; funding acquisition; investigation; methodology; resources. **Ahmed Abu-Dief:** Formal analysis; funding acquisition; investigation; methodology; resources; supervision; validation.

ORCID

Enas T. Aljohani  <https://orcid.org/0000-0001-9476-0892>

Mohamed R. Shehata  <https://orcid.org/0000-0003-1289-0285>

Fatmah Alkhatib  <https://orcid.org/0000-0003-1268-3075>

Seraj Omar Alzahrani  <https://orcid.org/0000-0001-7996-6593>

Ahmed M. Abu-Dief  <https://orcid.org/0000-0003-3771-9011>

REFERENCES

- [1] T. Thirunavukkarasu, H. A. Sparkes, K. Natarajan, V. G. Gnanasoundari, *Inorg. Chem. Acta* **2018**, 437, 255.
- [2] L. H. Abdel-Rahman, A. M. Abu-Dief, M. O. Aboelez, A. A. H. Abdel-Mawgoud, *J. Photochem. Photobiol. B* **2017**, 170, 271.
- [3] L. H. Abdel-Rahman, M. S. Adam, A. M. Abu-Dief, H. Moustafa, M. Basha, A. H. Aboria, B. S. Al-Farhan, H. El-Sayed Ahmed, *Appl. Organomet. Chem.* **2018**, 32, e4527.
- [4] A. M. Abu-Dief, H. M. El-Sagher, M. R. Shehata, *Appl. Organomet. Chem.* **2019**, 33, e4943.
- [5] A. M. Abu-Dief, L. H. Abdel-Rahman, A. A. Hassan Abdel-Mawgoud, *Appl. Organomet. Chem.* **2020**, 34, e5373.
- [6] T. K. Goswami, B. V. S. K. Chakravarthi, M. Roy, A. A. Karande, A. R. Chakravarty, *Inorg. Chem.* **2011**, 50, 8452.
- [7] M. Topçu Sulak, Ö. Gökdoğan, A. Gülce, H. Gülce, *Biosens. Bioelectron.* **2006**, 21, 1719.
- [8] C. Ornelas, *New J. Chem.* **2011**, 35, 1973.
- [9] F. Zhao, Z. Q. Liu, *J. Phys. Org. Chem.* **2009**, 22, 791.
- [10] A. M. Abu-Dief, I. F. Nassar, W. H. Elsayed, *Appl. Organomet. Chem.* **2016**, 30, 917.
- [11] O. N. Kadkin, G. Yu. Russ, *Chem. Rev.* **2012**, 81, 675.
- [12] C. Bizzarri, V. Conte, B. Floris, P. Galloni, *J. Phys. Org. Chem.* **2011**, 24, 327.
- [13] Y. Yuanyuan, *Synth. React. Inorg. Met. Org. Chem.* **2015**, 45, 1788.
- [14] B. Delavaux-Nicot, R. Mathieu, D. Montauzon, G. Lavigne, J. P. I. Majoral, *Inorg. Chem.* **1994**, 33, 434.
- [15] K. Tamas, B. Péter, S. Daniele, M. Giovanni, D. Patrick, *Inorg. Chim. Acta* **1995**, 239, 145.
- [16] S. A. Mohd Sukri, L. Y. Heng, N. H. Abd Karim, *J. Fluoresc.* **2017**, 27, 1,009.
- [17] A. M. Abu-Dief, L. A. E. Nassr, *J. Iran. Chem. Soc.* **2015**, 12, 943.
- [18] L. H. Abdel-Rahman, A. M. Abu-Dief, R. M. El-Khatib, S. M. Abdel-Fatah, *J. Photochem. Photobiol. B* **2016**, 162, 298.
- [19] L. H. Abdel-Rahman, A. M. Abu-Dief, M. R. Shehata, F. M. Atlam, A. A. H. Abdel-Mawgoud, *Appl. Organomet. Chem.* **2019**, 33, e4699.
- [20] A. M. Abu-Dief, L. H. Abdel-Rahman, M. R. Shehata, A. A. Hassan Abdel-Mawgoud, *J. Phys. Org. Chem.* **2019**, 32, e4009.
- [21] L. H. Abdel-Rahman, A. M. Abu-Dief, M. Ismael, M. A. A. Mohamed, N. A. Hashem, *J. Mol. Struct.* **2016**, 1, 232.
- [22] L. H. Abdel-Rahman, A. M. Abu-Dief, H. Mostafa, S. K. Hamdan, *Appl. Organomet. Chem.* **2017**, 31, e3555.
- [23] L. H. Abdel-Rahman, A. M. Abu-Dief, H. Moustafa, A. A. H. Abdel-Mawgoud, *Arab J Chem* **2020**, 13, 649.
- [24] L. H. Abdel-Rahman, A. M. Abu-Dief, R. M. El-Khatib, S. M. Abdel-Fatah, *Bioorg. Chem.* **2016**, 69, 140.
- [25] L. H. Abdel-Rahman Ahmed, M. Abu-Dief, R. M. El-Khatib, S. M. Abdel-Fatah, *Int. J. Nano. Chem.* **2018**, 4, 1.
- [26] L. H. Abdel-Rahman, R. M. El-Khatib, L. A. E. Nassr, F. E. D. Lashin, *Spectrochim. Acta a* **2013**, 111, 266.
- [27] L. H. Abdel-Rahman, A. A. Abdelhamid, A. M. Abu-Dief, M. R. Shehata, M. A. Bakhe, *J. Mol. Struct.* **2020**, 1, 127.
- [28] D. Sabolova, M. Kozurkova, T. Plichta, Z. Ondrusova, D. Hudecova, M. Simkovic, H. Paulikova, A. Valent, *Int. J. Biol. Macromol.* **2011**, 48, 319.
- [29] L. H. Abdel-Rahman, R. M. El-Khatib, L. A. E. Nassr, A. M. Abu-Dief, M. Ismael, A. S. Amin, *Spectrochim. Acta a* **2014**, 117, 366.
- [30] L. H. Abdel-Rahman, A. M. Abu-Dief, E. F. Newair, S. K. Hamdan, *J. Photochem. Photobiol. B* **2016**, 160, 18.
- [31] A. D. M. Mohamad, M. J. A. Abualreish, A. M. Abu-Dief, *J. Mol. Liq.* **2019**, 290, 162.
- [32] A. M. Abu-Dief, L. H. Abdel-Rahman, A. A. Abdelhamid, A. A. Marzouk, M. R. Shehata, M. A. Bakheet, O. A. Almaghrabi, A. Nafady, *Spectrochim. Acta a* **2020**, 228, 700.
- [33] Y. H. Zhang, J. C. Yuan, W. J. Lao, Y. Q. Yin, Z. X. Huang, J. J. Wu, *J. Organomet. Chem.* **2001**, 628, 123.
- [34] M. Bal, G. Ceyhan, B. Avar, M. Kose, A. Kayraldiz, M. Kurtoglu, *Turk. J. Chem.* **2014**, 38, 222.
- [35] a) I. Kashar, *Thermochim. Acta* **2010**, 507–508, 66; b) A. Elshafaie, L. H. Abdel-Rahman, A. M. Abu-Dief, S. K. Hamdan, A. M. Ahmed, E. M. M. Ibrahim, *Nano* **2018**, 13, 1850074; c) E. M. M. Ibrahim, L. H. Abdel-Rahman, A. M. Abu-Dief, A. Elshafaie, S. K. Hamdan, A. M. Ahmed, *Phys. Scr.* **2018**, 93, 055801.
- [36] N. Gupta, S. Chandra, *Spectrochim. Acta a* **2005**, 61, 1175.
- [37] I. Ali, W. A. Wani, K. Saleem, *Synth React Inorg Met Org Chem* **2013**, 43, 1,162.
- [38] a) L. H. Abdel-Rahman, A. M. Abu-Dief, M. S. S. Adam, S. K. Hamdan, *Catal. Lett.* **2016**, 146, 73; b) L. H. Abdel-Rahman, N. M. Ismail, M. Ismael, A. M. Abu-Dief, E. A.-H. Ahmed, *J. Mol. Struct.* **2017**, 1134, 851.
- [39] V. S. Elanchezhian, M. Kandaswamy, *Inorg. Chem. Commun.* **2009**, 12, 16.
- [40] N. A. El-Wakiel, *Appl. Organomet. Chem.* **2016**, 30, 664.
- [41] M. Gaber, H. A. El-Ghamry, S. K. Fathalla, *Spectrochim. Acta a* **2015**, 139, 396.
- [42] V. P. Tamilenth, *Arch. Appl. Sci. Res.* **2010**, 1, 57.
- [43] H. Katouah, A. M. Hameed, A. Alharbi, F. Alkhatib, R. Shah, S. Alzahrani, R. Zaky, N. M. El-Metwaly, *ChemistrySelect* **2020**, 5, 10256.
- [44] M. Montazerozhori, S. MojahediJahromi, A. Masoudiasl, P. McArdle, *Spectrochim. Acta a* **2015**, 5, 517.
- [45] S. S. Shah, R. G. Parmar, *Pharma Chem.* **2011**, 3, 318.
- [46] a) L. H. Abdel-Rahman, R. M. El-Khatib, L. A. E. Nassr, A. M. Abu-Dief, *Arab J Chem* **2017**, 10, S1835; b) S. I. Al-Saeedi, L. H. Abdel-Rahman, A. M. Abu-Dief, S. M. Abdel-Fatah, T. M. Alotaibi, A. M. Alsalmeh, A. Nafady, *Catalysts* **2018**, 8, 452.
- [47] M. S. S. Adam, O. M. El-Hady, F. Ullah, *RSC Adv.* **2019**, 9, 34311.
- [48] E. M. Zayed, M. A. Zayed, A. M. M. Hindy, G. G. Mohamed, *Appl. Organomet. Chem.* **2018**, 32, e4603.
- [49] L. H. Abdel-Rahman, M. S. Adam, A. M. Abu-Dief, H. E.-S. Ahmed, A. Nafady, *Molecules* **2020**, 25, 5089.
- [50] L. H. Abdel-Rahman, A. M. Abu-Dief, N. M. Ismail, M. Ismael, *Inorg. Nano-Met. Chem.* **2017**, 47, 467.
- [51] L. H. Abdel-Rahman, A. M. Abu-Dief, S. K. Hamdan, A. A. Seleem, *Int. J. Nano. Chem.* **2015**, 1, 65.

- [52] W. H. Mahmoud, R. G. Deghadi, G. G. Mohamed, *Arab. J. Chem.* **2020**, *13*, 5390.
- [53] S. Terpilowska, A. K. Siwicki, *Chem. Biol. Interact.* **2019**, *298*, 43.
- [54] A. Palanimurugan, A. Dhanalakshmi, P. Selvapandian, A. Kulandaisamy, *Heliyon* **2019**, *5*, e02039.
- [55] S. Shaaban, A. Negm, A. M. Ashmawy, D. M. Ahmed, L. A. Wessjohann, *Eur. J. Med. Chem.* **2016**, *122*, 55.
- [56] S. Chacko, S. Samanta, *Biomed. Pharmacother.* **2017**, *89*, 162.
- [57] F. Arjmand, S. Parveen, *RSC Adv.* **2012**, *2*, 6354.

SUPPORTING INFORMATION

Additional supporting information may be found online in the Supporting Information section at the end of this article.

How to cite this article: Aljohani ET, Shehata MR, Alkhatib F, Alzahrani SO, Abu-Dief AM. Development and structure elucidation of new VO^{2+} , Mn^{2+} , Zn^{2+} , and Pd^{2+} complexes based on azomethine ferrocenyl ligand: DNA interaction, antimicrobial, antioxidant, anticancer activities, and molecular docking. *Appl Organomet Chem.* 2021;35:e6154. <https://doi.org/10.1002/aoc.6154>